Computational Modelling of Human Electrophysiological Data

Von der Medizinischen Fakultät
der Rheinisch-Westfälischen Technischen Hochschule Aachen
zur Erlangung des akademischen Grades einer Doktorin der Theoretischen Medizin
genehmigte Dissertation

vorgelegt von

Master of Science

Anna Maxion

aus Aachen

Berichter: apl. Prof. Dr. med. Barbara Namer
Jun.-Prof. Dr. rer. nat. Jenny Tigerholm

Tag der mündlichen Prüfung: 07.11.2025

In der Dissertation enthaltene Publikationen:

A. Maxion, E. Kutafina, A. Fiebig, M. F. Dohrn, P. Sacré, A. Lampert, J. Tigerholm, B. Namer, A modelling study to dissect the potential role of voltage-gated ion channels in activity-dependent conduction velocity changes as identified in small fiber neuropathy patients. *Front. Comput. Neurosci.* **17**, (2023).

A. Maxion, A. J. Gaebler, R. Röhrig, K. Mathiak, J. Zweerings, E. Kutafina, Spectral changes in electroencephalography linked to neuroactive medications: A computational pipeline for data mining and analysis, Computer Methods and Programs in Biomedicine, Volume 255, 2024,108319, ISSN 0169-2607, https://doi.org/10.1016/j.cmpb.2024.108319.

frontiers | Frontiers in Computational Neuroscience

TYPE Original Research
PUBLISHED 14 December 2023
DOI 10.3389/fncom.2023.1265958

OPEN ACCESS

EDITED BY
Christian Leibold,
Ludwig Maximilian University of Munich, Germany

REVIEWED BY
Henrique Prado von Gersdorff,
Oregon Health and Science University, United States
Bruce Graham,
University of Stirling, United Kingdom

*CORRESPONDENCE
Anna Maxion
✉ anna.maxion@rwth-aachen.de

†These authors share last authorship

RECEIVED 24 July 2023
ACCEPTED 25 October 2023
PUBLISHED 14 December 2023

CITATION
Maxion A, Kutafina E, Dohrn MF, Sacré P, Lampert A, Tigerholm J and Namer B (2023) A modelling study to dissect the potential role of voltage-gated ion channels in activity-dependent conduction velocity changes as identified in small fiber neuropathy patients. *Front. Comput. Neurosci.* 17:1265958. doi: 10.3389/fncom.2023.1265958

A modelling study to dissect the potential role of voltage-gated ion channels in activity-dependent conduction velocity changes as identified in small fiber neuropathy patients

Anna Maxion[1]*, Ekaterina Kutafina[2], Maike F. Dohrn[3], Pierre Sacré[4], Angelika Lampert[5], Jenny Tigerholm[6†] and Barbara Namer[1,7,8†]

[1]Research Group Neuroscience, Interdisciplinary Centre for Clinical Research within the Faculty of Medicine at the RWTH Aachen University, Aachen, Germany, [2]Institute of Medical Informatics, Medical Faculty, RWTH Aachen University, Aachen, Germany, [3]Department of Neurology, Medical Faculty, RWTH Aachen University, Aachen, Germany, [4]Department of Electrical Engineering and Computer Science, University of Liège, Liège, Belgium, [5]Institute of Neurophysiology, Uniklinik RWTH Aachen University Aachen, Aachen, Germany, [6]Joint Research Center for Computational Biomedicine, RWTH Aachen, Aachen, Germany, [7]Institute of Neurophysiology, RWTH Aachen University, Aachen, Germany, [8]Institute of Physiology and Pathophysiology, University of Erlangen-Nürnberg, Erlangen, Germany

Objective: Patients with small fiber neuropathy (SFN) suffer from neuropathic pain, which is still a therapeutic problem. Changed activation patterns of mechano-insensitive peripheral nerve fibers (CMi) could cause neuropathic pain. However, there is sparse knowledge about mechanisms leading to CMi dysfunction since it is difficult to dissect specific molecular mechanisms in humans. We used an *in-silico* model to elucidate molecular causes of CMi dysfunction as observed in single nerve fiber recordings (microneurography) of SFN patients.

Approach: We analyzed microneurography data from 97 CMi-fibers from healthy individuals and 34 of SFN patients to identify activity-dependent changes in conduction velocity. Using the NEURON environment, we adapted a biophysical realistic preexisting CMi-fiber model with ion channels described by Hodgkin-Huxley dynamics for identifying molecular mechanisms leading to those changes. Via a grid search optimization, we assessed the interplay between different ion channels, Na-K-pump, and resting membrane potential.

Main results: Changing a single ion channel conductance, Na-K-pump or membrane potential individually is not sufficient to reproduce in-silico CMi-fiber dysfunction of unchanged activity-dependent conduction velocity slowing and quicker normalization of conduction velocity after stimulation as observed in microneurography. We identified the best combination of mechanisms: increased conductance of potassium delayed-rectifier and decreased conductance of Na-K-pump and depolarized membrane potential. When the membrane potential is unchanged, opposite changes in Na-K-pump and ion channels generate the same effect.

Significance: Our study suggests that not one single mechanism accounts for pain-relevant changes in CMi-fibers, but a combination of mechanisms. A depolarized membrane potential, as previously observed in patients with neuropathic pain, leads to changes in the contribution of ion channels and the

Na-K-pump. Thus, when searching for targets for the treatment of neuropathic pain, combinations of several molecules in interplay with the membrane potential should be regarded.

KEYWORDS

neuron, simulation, C-fiber axon, neuropathic pain, microneurography, voltage-gated ion channels, in-silico model

1 Introduction

Neuropathic pain affects 7–10% of the population and results from damage to the somatosensory system (Colloca et al., 2017; Petroianu et al., 2023). Factors such as an aging population, diabetes, and cancer treatment increase the incidence of neuropathic pain, which presents itself in a diverse array of manifestations. Small fiber neuropathy (SFN) is a medical condition that affects the small sensory cutaneous nerve fibers, such as Aδ and C-fibers (Sène, 2018; Strand et al., 2022). Common is a mechanically evoked hyperalgesia in the extremities (Serra et al., 2011; Chan and Wilder-Smith, 2016). However, for unknown reasons, not all patients with neuropathy experience pain. Unfortunately, up to now, there is no biomarker for ongoing pain in patients with SFN. Identifying a reliable assessment of excitability alterations in patients is important for understanding the pathophysiological mechanisms underlying neuropathic pain and why some patients develop pain while others do not.

Voltage-gated sodium channels (Na_v) play an important role in pain signaling as shown by monogenic diseases affecting pain sensitivity ranging from insensitivity to pain to extreme painful disorders such as paroxysmal pain disorder (Habib et al., 2015; Bennett et al., 2019; Körner and Lampert, 2020; Goodwin and McMahon, 2021). SFN can be associated with gene variants in the genes of the subtypes $Na_v1.7$, $Na_v1.8$, or $Na_v1.9$ (Huang et al., 2014; Chan and Wilder-Smith, 2016). Thus, the function of voltage-gated sodium channels, especially of the subtypes $Na_v1.7$, $Na_v1.8$, and $Na_v1.9$ are prone candidates to account for differences between patients with or without ongoing neuropathic pain. However, also other membrane properties and molecules such as resting membrane potential (RMP), sodium potassium pump (Na-K-pump), or voltage-gated potassium channels modulate the excitability of the membrane and thus can play a critical role in ongoing neuropathic pain (Burke et al., 2001; Krishnan et al., 2008; Busserolles et al., 2016).

Microneurography allows to assess the conduction of nerve signals (action potentials) in peripheral nerve fibers in healthy human volunteers, as well as in diseased patients with neuropathic pain. With this method, the response of single unmyelinated nerve fibers (C-fibers) to electrical stimuli can be recorded and mechano-sensitive (CM) or mechano-insensitive (CMi) fibers can be identified. In this study, we are focusing on CMi-fibers which become hyperexcitable and spontaneously active in patients with diabetic neuropathy and erythromelalgia correlating to the presence of ongoing pain (Kleggetveit et al., 2012).

During microneurography, the receptive field of the C-fibers is stimulated with electrical, mechanical, or chemical stimuli, which results in the creation of action potentials that travel from the stimulation site to the recording electrode. The corresponding delay between stimulation and recording time is called latency and increases for higher frequencies of electrical stimulation, i.e., the response of the fiber becomes slower and is therefore referred to as activity-dependent slowing (ADS). Reducing the frequency of the stimulation leads to a return of the latency to its baseline level, i.e., normalization of latency (Schmelz et al., 1995; Weidner et al., 1999).

When assessing pain patients using microneurography, several changes in the activity-dependent conduction velocity were found, when compared to healthy volunteers. An erythromelalgia patient with a gain-of-function mutation in $Na_v1.7$ (I848T) showed frequency-dependent speeding of conduction velocity instead of slowing, as compared to the healthy control group (Namer et al., 2015). Another erythromelalgia patient with a mutation in $Na_v1.8$ exhibited an exaggerated ADS (Kist et al., 2016). In (Namer et al., 2009), healthy elderly volunteers expressed more ADS than younger subjects, as well as a slower normalization of latency after stimulation. However, the normalization of latency is quicker for SFN patients with pain than for those without pain (Kleggetveit et al., 2012).

ADS is enhanced by the slow inactivation of Na_vs (De Col et al., 2008) and intracellular sodium accumulation (Tigerholm et al., 2014). Thus, a faster normalization of latency could indicate that sodium channels emerge faster from slow inactivation, leading to a reduced time until the possible initiation of the next action potential, supporting higher overall excitability of the cell and higher discharge rates (De Col et al., 2012). However, it is unknown which ion channel subtypes or other mechanisms, such as Na-K-pump activity and RMP, contribute to enhanced excitability in neuropathic pain patients.

Due to ethical concerns, certain experimental procedures or pharmacological manipulations cannot be performed in microneurography in humans. Thus, to explore the mechanisms underlying changes in ADS and the normalization processes of ADS computational model systems are needed. The use of animal models is limited since specific types of nerve fibers, such as CMi-fibers, are absent in the skin of rodents (Prato et al., 2017). To overcome these limitations, we used a computational model (Tigerholm et al., 2014) based on microneurographic recordings in humans to simulate the activity of nerve fibers following electrical stimulation to study the mechanisms underlying quicker normalization in pain vs. non-pain SFN patients. We modulated the conductance of the sodium and potassium ion channels, as well as the Na-K-pump and RMP to assess their importance for the normalization of latency.

2 Methods

2.1 Computational model

We adapted the computational model of a C-fiber described by (Tigerholm et al., 2014). The reproduction of the specific behavior of

C-fibers of the model was verified several times by different authors (Petersson et al., 2014; Tigerholm et al., 2015; Pelot et al., 2021). The Hodgkin-Huxley-type biophysical model was originally implemented using the NEURON simulation environment (Hines and Carnevale, 1997) and its built-in interpreter *hoc* with a MATLAB interface for controlling the simulation and plotting the data. We transferred the model to Python (version 3.11.1), which can be utilized as an interpreter for NEURON (Hines et al., 2009). NEURON was used in version 7.8. The code of the model can be accessed at GitHub (Maxion, 2023). One of the main advantages of using Python is the ability to run and evaluate the simulation within the same environment, streamlining the workflow and increasing efficiency. Originally, the multi-compartmental model consisted of a parent axon connected to a thinner branch axon with different diameters and temperatures. To be able to run extensive parameter searches we simplified the model reducing the fiber length to 1 cm with 600 compartments of uniform temperature (37°C) and diameter (1 µm), which lowered computation time by a factor of 10. The model includes three different sodium channels, Na_v 1.7, Na_v 1.8, and Na_v 1.9, each with an activation gate, a fast inactivation and a slow inactivation gate. The channel Na_v 1.8 additionally contains an ultra-slow inactivation gate. Further, four potassium channels are included. The delayed rectifier K_{dr} with an activation gate, the channel K_f with an activation and inactivation gate, the channel K_s with a fast and slow gate that are combined with factors such that the slow effect makes ¼, while the fast effect makes ¾ of the total effect, and the channel K_{Na} with one gate assuming that the opening of the gate is immediately affected by the concentration of sodium within the axon. Additionally, there is a hyperpolarization-activated channel *h* with a fast and a slow activation gate (also known as HCN). The included sodium and potassium leak currents are essential for maintaining a stable resting membrane potential (RMP) by ensuring that the total inward and outward currents carried by sodium and potassium ions are equal at rest. The Na-K-pump maintains the electrochemical gradient across the cell membrane. Further, the model allows dynamic changes in sodium and potassium concentrations. The underlying differential equations are solved using the variable timestep method.

2.2 Recording technique and subjects

With the method of microneurography nerve signals are recorded from single C-fibers. An uninsulated microelectrode of 0.005 mm at the tip is inserted into the nerve bundle of the superficial peroneal nerve at ankle level and a reference electrode is situated superficially in the skin close by (Figure 1). Regular electrical pulses, usually ¼ Hz, from an insulated constant current stimulator (Digitimer DS7, Digitimer, Hertfordshire, UK) are applied to the receptive field of the fibers and transmitted through superficially inserted electrodes. This stimulation triggers a response from the fibers in the form of action potentials that occur at a consistent latency, allowing for the identification of multiple fibers within the same recording. Fiber properties such as the mechanical threshold of individual fibers are evaluated using the marking method (Torebjörk and Hallin, 1974; Schmidt et al., 1995). The stimulation as well as the recording of the fiber activity are conducted in DAPSYS (Data Acquisition Processor System (DAPSYS), Brian Turnquist, http://dapsys.net), a system that acquires and processes data in real-time.

Microneurography data, obtained from 97 mechano-insensitive C-fibers (CMi) of healthy individuals, which has been collected and aggregated in our database since 2004, was utilized to validate the representation of CMi-fiber in the computational model. Two fibers had to be excluded from the dataset. One because of incomplete data, due to recording issues and the other fiber was excluded because it was misclassified in the original data set, leading to 95 fibers (Table 1).

Additionally, we examined small fiber neuropathy (SFN) patients in our laboratory to specifically investigate potential differences between patients experiencing pain in the foot or leg and those who did not. The study encompassed 142 nerve fibers from 19 patients in the age range of 23 to 59 years (mean age: 42.8 years), including 11 males and 8 females. For 129 of these fibers the ELID stimulation

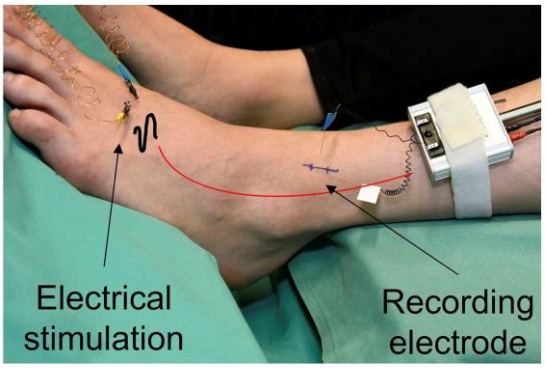

FIGURE 1
Nerve signals are recorded from single C-fibers. A microelectrode is inserted into the nerve bundle of the superficial peroneal nerve at ankle level (recording electrode). Regular electrical pulses from a constant current stimulator are applied to the receptive field of the fibers, transmitted through superficially inserted electrodes (electrical stimulation).

TABLE 1 Total number of fibers and number of CMi-fibers for the ELID stimulation protocol before and after exclusion of data that did not meet the inclusion criteria, the corresponding number of patients, and the number of males and females for healthy subjects and SFN patients with and without pain.

	Number of all fibers/ Number of patients	Number of CMi-fibers/ Number of patients	Number of CMi-fibers after exclusion/Number of patients
Healthy	337/-	97/-	95/-
SFN - total	129/19 (m:11, f:8)	34/13 (m:7, f:6)	32/13 (m:7, f:6)
SFN - pain	66/9 (m:4, f:5)	25/6 (m:3, f:3)	23/6 (m:3, f:3)
SFN – no pain	63/10 (m:7, f:3)	9/7 (m:4, f:3)	9/7 (m:4, f:3)

protocol was performed (Table 1). Some of the fibers showed spontaneous activity, while others did not. Of these fibers, 34 were classified as CMi-fibers according to their receptive properties such as mechanical threshold and response to electrical stimulation. Patients who were classified without pain reported no pain in the foot, where the data was recorded, but experienced pain in other parts of the body. Two fibers were excluded from further analysis, because they showed branching behavior, i.e., one branch of the fiber blocks, which leads the electrical signal being transmitted by another branch of the fiber. This leads to large sudden changes in latency. After excluding incomplete data, 32 CMi-fibers from 13 patients were left. These fibers consist of 9 fibers from 7 patients without pain and 23 fibers from 6 patients with pain at the recording position, i.e., the foot. To compare the different groups statistically, the data sets were checked visually for normal distribution, which was not present. Therefore, a Kruskal-Wallis test with a significance level of $\alpha = 0.05$ was used to compare healthy individuals and SFN patients with pain and without pain. For the *post hoc* pairwise comparison of the groups, a Wilcoxon rank sum test was utilized. To correct for multiple comparisons, we applied a Bonferroni correction with a significance level of $\alpha/3 = 0.017$. The statistical analysis was conducted in Python (version 3.11.1).

The collection of the data was approved by the local ethics committees from Aachen (EK 141/19) and Erlangen (4361) and conducted in accordance with the principles embodied in the Declaration of Helsinki and statutory requirements of Germany. All participants gave written informed consent to participate in the study.

2.3 Stimulation protocol

After a rest period of at least 2 min, the fibers were stimulated with electrical square pulses of 0.5 ms duration of rising frequencies of 1/8 Hz (20 pulses), 1/4 Hz (20 pulses), and 1/2 Hz (30 pulses) and normalization of latency is observed with a frequency of ¼ Hz for at least 10 pulses. The well-known stimulation protocol is used to identify different fiber types, such as mechano-sensitive (CM) and mechano-insensitive (CMi) C-fibers, and therefore called ELID (electrical identification; Weidner et al., 1999).

2.4 Defining parameters

During ongoing stimulation, the latency, i.e., the time an action potential needs to travel from the point of stimulation to the point of measurement, increases for stimulation with higher frequencies and decreases, if the frequency is lowered. Those changes in response latency are called activity-dependent slowing (ADS). The latency was measured in relation to the initial latency and the maximum ADS (ADS_{total}) was calculated (Figure 2, left). Additionally, the normalization of latency during stimulation with a lower frequency was measured in relation to the total slowing (ADS_{total}) to make the normalization comparable for fibers with different total ADS (Figure 2, right). Here, the total recovery (rec_{total}) was used for evaluation.

2.5 Method of identifying relevant mechanisms

To implement a computational model that evaluates differences between SFN patients with and without pain, several parameter optimization steps were pursued. The ADS of pain and non-pain patients is similar (pain patients: 7.93% ± 1.36%, non-pain patients: 7.6% ±0.47%, difference: 0.33%), while the normalization of latency is statistically significantly faster for pain patients (pain patients: 75.8% ±9.4%, non-pain patients: 84.6% ±3.2%, difference: −8.8%) for the given protocol (Kleggetveit et al., 2012). An overview of the performed workflow is shown in Figure A1 in the Supplementary Figures and in the following each step is explained in detail.

In the first step, the conductance levels of the ion channels and the Na-K-pump rate, i.e., the conductance of the Na-K-pump, were modulated systematically by increasing and decreasing each level individually by 25% and 50% of its original value independently from each other. The maximal change of 50% was chosen to preserve the original ADS of the fiber. Higher deviations from the original value led to large changes in ADS and could therefore not replicate the desired result. In the model the initial RMP is set at the beginning of each simulation. Changes in the behavior of ion channels, i.e., the conductance, or the Na-K-pump do not affect the initial RMP, unlike in a real fiber. Therefore,

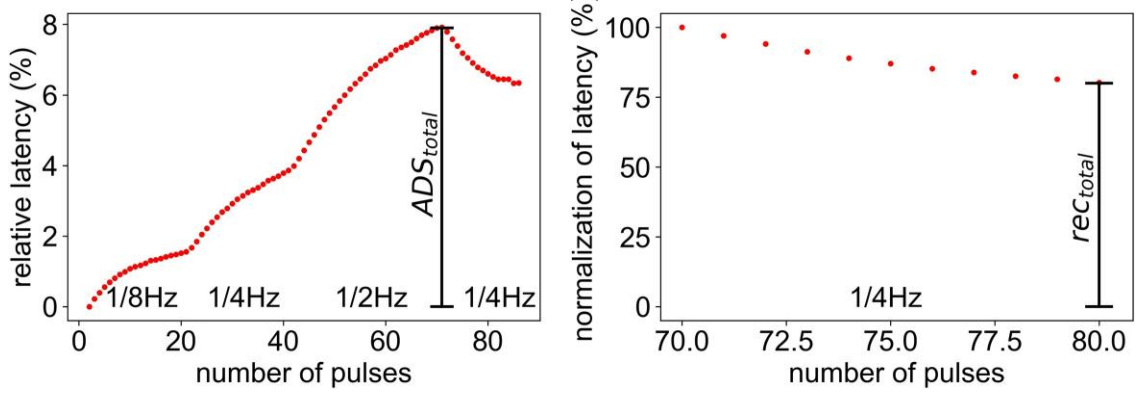

FIGURE 2
Measurement of ADS_{total} and rec_{total} for the ELID stimulation protocol. (Left) latency relative to initial latency. ADS_{total} represents the maximal ADS after high frequency stimulation. (Right) Normalization of latency after the stimulation. The last 10 values of the relative latency (Left) are divided by ADS_{total}. rec_{total} represents the amount of total recovery after 10 pulses during low frequency stimulation.

the initial RMP was de- and hyperpolarized by 5mV (original: −55 mV) separately from the other changes to be able to replicate the behavior of a real fiber more accurately. The computational model was evaluated for each individual variation of conductance level, Na-K-pump rate and RMP and the values ADS_{total} and rec_{total} were calculated.

Further, we combined the individual variations of conductance levels, Na-K-pump rate and RMP by adding the values ADS_{total} and rec_{total} for all existing combinations. For example, for a 50% decreased pump rate the model shows an increased value of ADS_{total}, while for a depolarized RMP the model shows a decreased value of ADS_{total} . If the two models are combined the effects cancel each other out and the ADS_{total} in the combined model is near zero. Thus, we could calculate the combined values without needing to evaluate the computational model for each combination. We evaluated which combinations led to a faster normalization of latency, i.e., a smaller value of rec_{total} by −8.8%±0.7%, while simultaneously having only a minor effect on the overall slowing ADS_{total} of 0.33% ± 0.7%. The 0.7% was added as an error margin. From the resulting combinations, we chose the ones where three or less mechanisms were modulated and executed the model with these parameters. In the resulting simulation data, we measured again ADS and normalization of latency and compared them for each parameter set. We chose the parameter sets where the absolute difference in ADS was below 1% and the difference in normalization of latency was in the interval of [−8.8–4.5%, −8.8+4.5%], since the normalization showed a larger variation in the data of SFN patients.

2.6 Grid search

Further, we used an algorithm for parameter optimization based on grid search. This method exhaustively tries every combination of the specified parameter values, i.e., conduction of ion channel, Na-K-pump rate, and RMP, in a predefined grid. We chose a grid of five values for the ion channels and the Na-K-pump (−50, −25%, original, +25%, +50%) and three values for the RMP (−5 mV, original, +5mV) and evaluated the computational model at each point. This allowed us to explore a wide range of possible combinations of conductance values for the selected mechanisms. To reduce the runtime of the grid search, we selected three mechanisms for each run that showed the desired behavior in the previous analysis. The performance of each model was evaluated by comparing the ADS_{total} and the normalization of latency rec_{total} with the desired values of 0.33 for ADS and −8.8% for normalization of latency. To ensure that the perturbation of parameters results in a valid model that preserves the original properties of the in-silico fiber, the spike shape, gating variables and the ionic currents were reviewed visually. For each grid search the model that was closest to these values was chosen. Lastly, the model was run with the optimized parameter sets to verify the result.

3 Results

3.1 The adapted model resembles CMi-fibers in activity-dependent conduction velocity changes

To calibrate our computer model to mimic the behavior of healthy human CMi-fibers, we analyzed data recorded from 95 CMi-fibers from healthy subjects using the ELID frequency protocol (indicated by grey markers in Figure 3). In Figure 3, we included 85 CM-fibers (represented by black markers) for comparison purposes, highlighting the more pronounced ADS of the CMi-fibers within this large dataset. In a first step, we aim to determine the neurite diameter of the simulated nerve fibers which produces ADS best fitting to CMi-fibers. We compared the simulated data from the presented computational model (see methods) for four diameters with the data collected from human healthy subjects (Figure 3). For a diameter of 1 µm, the result of the computational model is consistent with electrically stimulated conduction velocity changes of CMi-fibers of healthy volunteers.

3.2 Normalization of latency is faster for pain patients

In this study we are analyzing a large data set of CM and CMi-fibers of 19 SFN patients (substantially larger than those reported before (Kleggetveit et al., 2012)), providing a solid basis for computational modeling. We focused on ADS, relative latency, and normalization of latency in SFN patients with and without pain compared to healthy volunteers (Figures 4A,B). ADS_{total}, the maximal latency observed for CMi-fibers, is similar for all groups (pain: 7.97%±0.51%, no pain: 8.32%±0.74%, healthy: 7.91%±0.24%, p-value = 0.811). In contrast, the normalization of latency is significantly quicker for the SFN patients with pain compared to those without or the healthy controls (pain: 70.89% ± 2.4%, no pain: 78.75%±4.17%, healthy: 78.93%±1.29%, p-value=0.008). The post-hoc analysis showed that this difference is only significant between patients with pain and healthy subjects (p-value = 0.002), whereas the difference between patients with and without pain shows a tendency (p-value=0.107). It has to be noted, that there were only a few no-pain patients (n=9) because most SFN patients have ongoing pain in their extremities. Patients without pain and healthy subjects showed very similar behavior (p-value = 0.849). Note that the statements regarding significance for the post-hoc analysis consider a

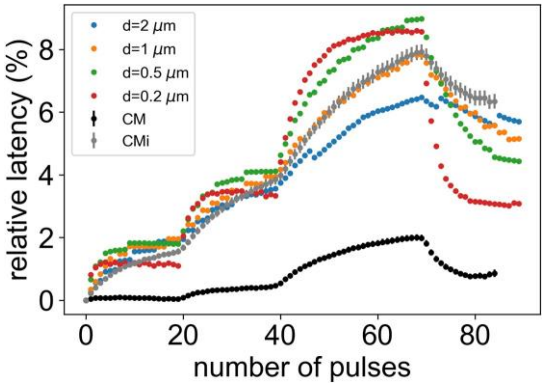

FIGURE 3
Comparison of microneurography data for CM- and CMi-fibers from healthy subjects with simulation data for different diameters. The error bars show the standard error of the mean. The CM-fiber is added for comparison to provide a basis for better judgment of the variance of different fiber diameters.

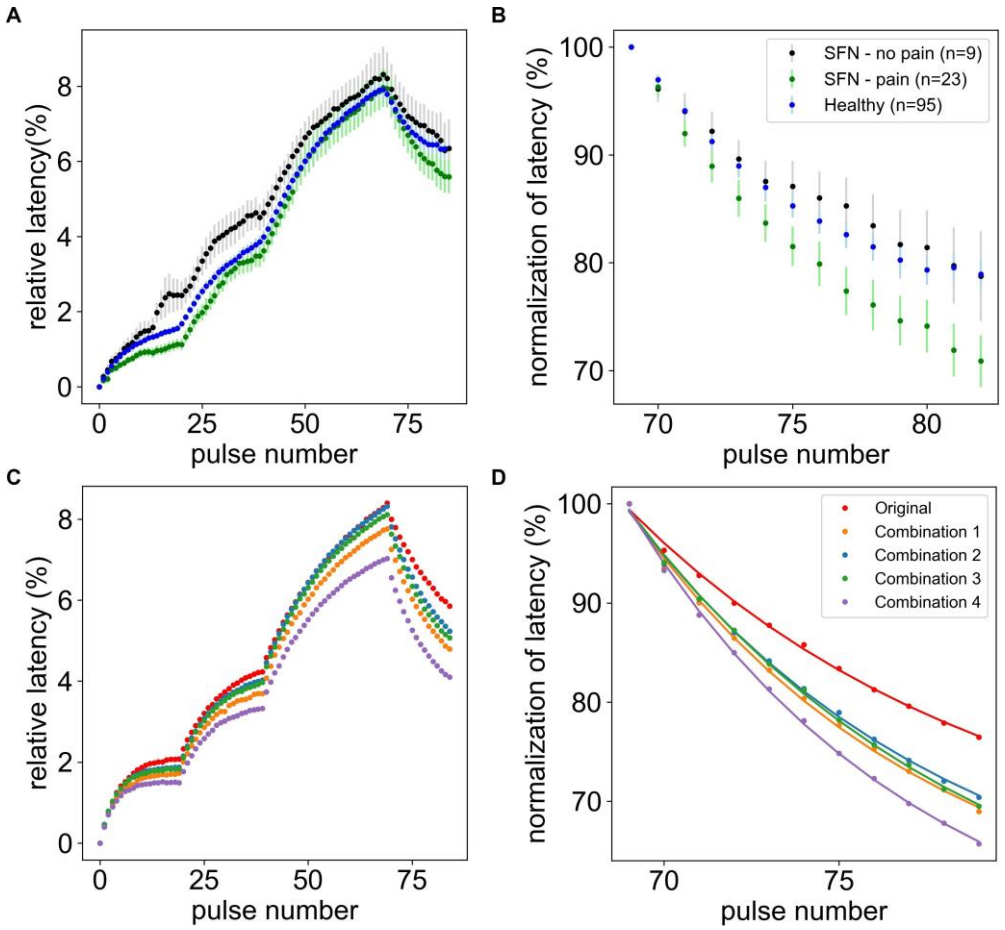

FIGURE 4
Comparison of microneurography data and simulated data. The upper panels show the mean and standard error of the mean of the relative latency of the full frequency protocol **(A)** and normalization of latency after stimulation **(B)** for healthy subjects (n = 95), pain (n = 23), and non-pain (n = 9) SFN patients. The lower panels show the best simulation results after the grid search compared to the original model (red) for the full frequency protocol **(C)** and normalization of latency after stimulation **(D)**. In combination 1 the channel is increased by 50% and the Na-K-pump is increased by 37.5%. In combination 2 the channel is increased by 37.5% and the channel h is reduced by 50%. In combination 3 the channel is increased by 50%, the Na-K-pump is reduced by 25% and the RMP is depolarized. In combination 4 the channel is increased by 50%, the channel h is increased by 50% and the RMP is depolarized.

Bonferroni correction for multiple testing, leading to a significance level of $\alpha = 0.017$ for comparison with the p-values.

3.3 Computational model: modulation of individual parameters

Now that we have identified significant differences in normalization of latency between patients with pain and healthy controls, we can use this data to optimize our model and investigate the possible underlying conductances for enhanced or decreased ADS or the speed of normalization. Using the computational model introduced in the methods, we explored how changes in the conductance of all ion channels, the Na-K-pump rate, and the resting membrane potential (RMP), affect the maximal ADS_{total} and the total normalization of latency rec_{total}. The simulation results presented in Figure 5 show an example of this modulation for the Na-K-pump. It can be observed that, although an increasing Na-K-pump rate leads to a faster normalization of latency, simultaneously the ADS also changes substantially. Therefore, this variation did not improve the model.

3.3.1 Na-K-pump, RMP, and K_{dr} strongly affect ADS

ADS_{total} is mostly affected by changes in the Na-K-pump rate, the conductance of the potassium channel K_{dr} and the RMP (Figure 6). An increase of the Na-K-pump rate as well as a depolarization of RMP leads to a reduced ADS_{total}, while increasing conductance of $Na_v1.8$, K_{dr} and h has the opposite influence. The other channels only have a very slight impact on ADS_{total}, while surprisingly Na_v 1.9, as a large persistent current, seems not to be relevant for the effect of ADS for this low frequency stimulation protocol.

3.3.2 Normalization of latency is strongly influenced by the Na-K-pump, RMP and the hyperpolarization-activated current h

The simulation results and calculation of rec_{total}, shown in Figure 6, indicate that the Na-K-pump rate, the hyperpolarization-activated current h, and RMP have the most pronounced influence on the normalization of latency.

An increase in Na-K-pump rate or depolarization of RMP, as well as a decrease in the conductance of h, can lead to a faster

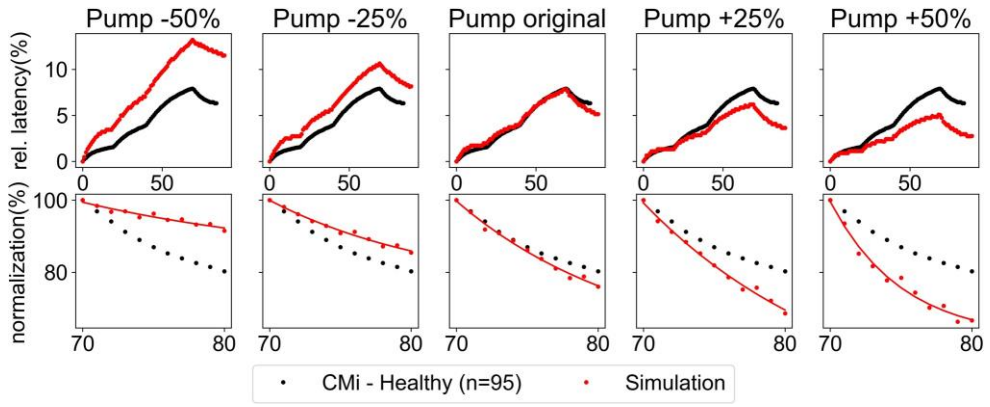

FIGURE 5
Variation of the Na-K-pump rate by ±25% and ±50% for the low protocol. Comparison of simulated data (red) and recorded data (black) of CMi-fibers from healthy subjects. The recorded data shows the mean and the standard error of the mean. Upper panel: relative latency for the full stimulation protocol. Lower panel: normalization of latency during the last ten pulses.

normalization. But these mechanisms reduce at the same time the ADS_{total}, which in pain patients is not different in comparison to healthy subjects. Further, increasing the conductance of the potassium channel K_s, as well as reducing the conductance of the hyperpolarization activated current h, the potassium channel K_{Na} or the sodium channels Na_v 1.7 or Na_v 1.8 also lead to a faster normalization, but to a smaller extent. Interestingly, different subtypes of one channel family, e.g., potassium channels, can have opposing effects on normalization. For example, a reduction of K_s conduction leads to a slower normalization, while a reduction of K_{Na} conduction results in a faster normalization. Thus, a very detailed analysis is important to understand C-fiber function.

3.3.3 Adding the effects of individual mechanisms

Since no single mechanism can recreate all observed differences between SFN patients with pain and healthy subjects, we assessed different combinations of multiple mechanisms. Hence, we combined all possible variations of conductance levels, Na-K-pump rate, and RMP, which led to a total of 11,648 possible combinations. To run the model for all combinations is too computationally demanding, therefore for each combination we calculated the combined ADS and recovery from the previously calculated values ADS_{total} and rec_{total} of the individual variations (Figure 6). Among these combinations were 18 that were able to reproduce the effect of unchanged ADS and faster normalization of latency. There was only one combination, where only two mechanisms were involved ($Pump + 25\%, K_{dr} + 25\%$) and 17 combinations where three mechanisms were involved. Eight of those 17 combinations consisted of $Pump + 25\%$ and $K_{dr} + 25\%$ and one other ion channel ($Na_v 1.7, Na_v 1.9, K_f, K_{Na}$) that had a negligible effect on the outcome. Therefore, we concluded that the main effect in these cases could be attributed to the Na-K-pump and K_{dr} and thus summarize these combinations in the combination $Pump + 25\%, K_{dr} + 25\%$. The remaining combinations can be found in Table 2.

Since the mechanisms influence each other, e.g., sodium influx influences the Na-K-pump rate, the identified combinations only give a rough indication of the optimal results. Therefore, the model was run with these 10 candidates of parameter sets and the result was compared to the original model (Figure A2 in Supplements). It can be observed that for some combinations the influence of the mechanisms on each other worsened the result for ADS and normalization of latency, i.e., some combinations have less ADS than the original, while others do not have a faster recovery. In Table 2 the exact numbers for the difference in ADS and normalization of latency compared to the original model are shown.

To find the best parameter sets, we need to look for those which have the lowest difference in ADS while simultaneously having a large difference in the normalization of latency. Therefore, the optimal parameter sets are numbers 1, 2, 5, and 6, marked in grey in Table 2.

3.4 Simultaneous modulation of multiple parameters within the computational model

To comprehend the interplay between ion channels, Na-K-pump, and RMP in greater depth, a grid search was performed for each of the four best combinations of mechanisms determined in the previous section. This approach additionally reveals mechanisms that have a negligible effect on ADS and latency normalization and identifies alternative parameter values for improved results. When visually inspecting the spike shapes of each resulting model, we found that seven models could not reproduce the original spike shape appropriately, see Figure A7, and were therefore excluded from further analysis. Further, it was confirmed that all gating variables reached steady state before the stimulation protocol starts.

3.4.1 The potassium channel K_f has low influence on ADS and normalization of latency

The results of the grid search for the ion channels K_{dr}, h, and K_f are depicted in Figure 7A. The colored lines corresponding to variations in the conductance of K_f exhibit a minimal difference in terms of ADS and normalization of latency. Therefore, the effect of K_f is low and its conductance can be maintained at its original value.

FIGURE 6
Effect of changing conductance of ion channels, Na-K-pump rate, and RMP of ADS on the left and normalization of latency on the right for a low-frequency protocol. The decrease/increase is shown in relation to the parameter value in the original model.

Further, h and K_{dr} influence each other, i.e., an increase in conductance of h results in a steeper line, indicating that variations in K_{dr} conductance have a greater effect on ADS for higher conductance of h. Conversely, variations in conductance of h also have a larger effect for higher conductance of K_{dr} (see Figure A3 in Supplements, here the lines are more dispersed for higher values of K_{dr} conductance). However, no clear interaction between K_{dr} and h is evident in the normalization of latency, see Figure 7A. The dashed line in the figures represents the optimal values for ADS and normalization of latency to match the behavior observed in SFN patients with pain (Kleggetveit et al., 2012), which is characterized by an increase in ADS by 0.33% and reduction in normalization by 8.8%. Therefore, in an optimal parameter set ADS and latency normalization should be simultaneously close to the dashed line, which is achieved by

TABLE 2 Channel combinations, where the ADS is similar to the original model, while the normalization of latency is faster.

No.	Channel combinations	ADS difference to original model in % (absolute value)	Normalization difference to original model in %
1	$Kf-50\%, K_{dr}+25\%, h-50\%$	0.42	−10.21
2	$Na_V1.7+25\%, K_{dr}+50\%, h-50\%$	0.45	−6.79
3	$Pump-50\%, h-50\%, RMP+5mV$	0.47	−0.05
4	$Pump+25\%, K_{dr}+25\%$	0.60	−3.81
5	$Pump-25\%, K_{dr}+25\%, RMP+5mV$	0.61	−6.65
6	$K_{dr}+50\%, h+50\%, RMP+5mV$	0.88	−12.90
7	$Pump+50\%, Na_V1.7+25\%, K_{dr}+50\%$	1.46	−9.23
8	$Pump-25\%, Na_V1.7-50\%, RMP+5mV$	1.60	−8.23
9	$Pump-25\%, K_{Na}+25\%, RMP+5mV$	1.70	−6.62
10	$Pump-25\%, Na_V1.7+50\%, RMP+5mV$	1.81	−7.11
	Experimental Data in Pain Patients (mean)	0.33	−8.8

Values for the difference in ADS and normalization of latency of channel combinations in comparison to the original model in ascending order for ADS. The goal is to have a low difference in ADS (<1%) and a faster normalization (in the range of −8.8%±4.5%). The fields in grey contain the combinations with the best fit.

reducing the conduction of h by 50% and increasing the conduction of K_{dr} by 37.5% (combination 2 in Figures 4, 8). Note that the optimal value for K_{dr} is in between the calculated values. Since the behavior of the simulated fiber for ADS and normalization of latency is in this case almost linear, we can still conclude that this value would be optimal for K_{dr}.

3.4.2 The sodium channel Na_V 1.7 does not influence ADS and normalization of latency

The findings of the grid search for the channels K_{dr}, h, and Na_V 1.7 are illustrated in Figure 7B. Similar to the previous grid search, it is visible that Na_V 1.7 conduction has no effect on ADS or latency normalization and its variations can be disregarded. This leads to the same optimal parameter combination as in the previous section, where conduction of h is reduced by 50% and K_{dr} conductance is increased by 37.5% (combination 2 in Figures 4, 8), and the prior observations about the influence of K_{dr} and h on each other hold true in this scenario as well.

3.4.3 The ion channels K_{dr} and h and RMP strongly influence ADS and latency normalization

The results of the grid search for the channels K_{dr}, h, and the RMP are depicted in Figure 7C. Both channels and the RMP have a noticeable effect on ADS and latency normalization unlike in the previous grid searches. For increased conductance of h variations in K_{dr} conductance affect the ADS more, which can be observed through increasingly steeper lines. Interestingly, variations in conductance of h only affect ADS and normalization when the RMP is maintained at its original value. On the other hand, variations in conductance of K_{dr} have a slightly more pronounced effect on ADS, if the RMP is hyperpolarized, which can be best observed Figure A5 in Supplements, where the steepness of the lines increases for hyperpolarized RMP. Two options for achieving an unchanged ADS and increased normalization as observed in pain patients can be identified. The first option involves retaining the RMP at its initial value, increasing K_{dr} conduction by 37.5% and simultaneously reducing h conduction by 50%, resulting in the same parameter set as previously identified in both prior grid searches (combination 2 in Figures 4, 8). The second option involves depolarizing the RMP by 5 mV, increasing h conduction by 50% and K_{dr} conduction by 50% (combination 4 in Figures 4, 8). Note that depolarizing the RMP leads to an increase in h conduction instead of a decrease.

3.4.4 The potassium channel K_{dr}, the Na-K-pump and RMP influence ADS and latency normalization

The results of the grid search modulating the parameters K_{dr}, the Na-K-pump and the RMP are depicted in Figure 7D. A reduction in Na-K-pump rate leads to an amplified effect of K_{dr} conduction and RMP on ADS, as seen in Figure 7D as increased dispersion of the lines and steeper lines for lower Na-K-pump rate. However, this effect is not reflected in the normalization of latency, where the dispersion and steepness of the lines is similar for all values of the Na-K-pump rate. Further, an increase in K_{dr} conduction results in a slightly larger influence of variations of the Na-K-pump rate on both the ADS and normalization as demonstrated in Figure A4 in the Supplements, where the dispersion of the lines is slightly larger. A hyperpolarization of RMP results in a heightened effect of both K_{dr} conduction and the Na-K-pump rate on the ADS as depicted in Figure A5 of the Supplements. Based on this grid search, two options for parameter sets have been identified that achieve our desired effect of unchanged ADS and reduced normalization of latency. For a depolarized RMP the optimal approach is to increase K_{dr} conduction by 50% and decrease the Na-K-pump rate by 25% (combination 3 in Figures 4, 8). For an unchanged RMP, a 37.5% increase of the Na-K-pump rate achieves the desired effect (combination 1 in Figures 4, 8), which can be best observed in Figure A5 in the Supplements. It needs to be noted that the

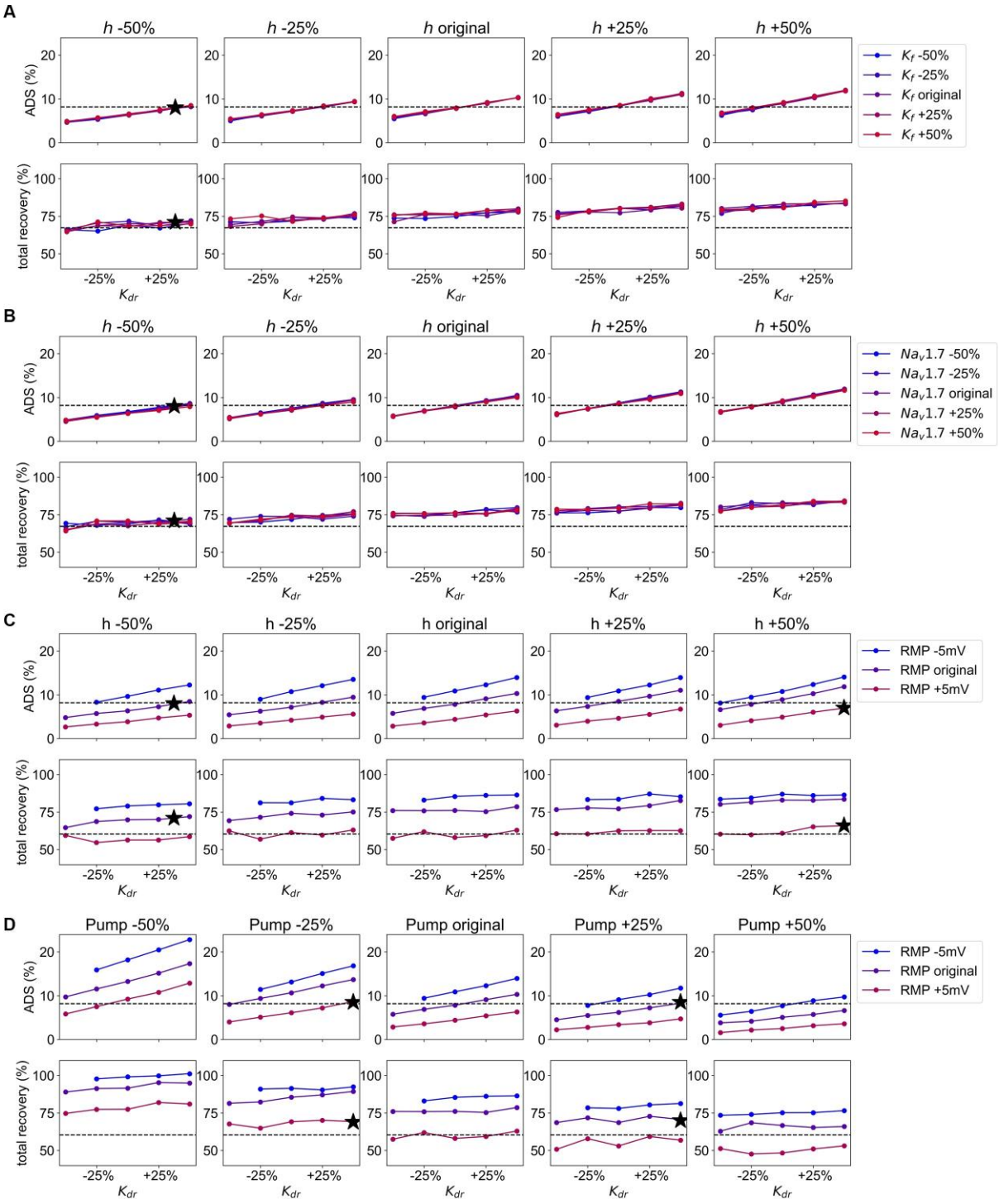

FIGURE 7
(A) Grid Search for the channels K_{dr}, h, and K_f. Values for K_{dr} are given on the x-axis, from the left panel to the right conduction of h is increasing, and the increasing values for K_f conduction are given in different colors from blue (decreased) to red (increased). The dotted line gives the value for ADS and normalization of latency, respectively as observed in pain patients. The black stars represent the optimal combination most similar to the values of ADS and normalization of latency in pain patients. Upper panel: the values for ADS for the model output with given parameter combinations. Lower panel: the values for normalization of latency for the model output with given parameter combinations. **(B)** Grid Search for the channels K_{dr}, h, and $Na_V1.7$. Values for K_{dr} are given on the x-axis, from the left panel to the right conduction of h is increasing, and the increasing conduction of $Na_V1.7$ is given in different colors from blue (decreased) to red (increased). The dotted line gives the value for ADS and normalization of latency, respectively as observed in pain patients. The black stars represent the optimal combination most similar to the values of ADS and normalization of latency in pain patients. Upper panel: the values for ADS for the model output with given parameter combinations. Lower panel: the values for normalization of latency for the model output with given parameter combinations. **(C)** Grid Search for the channels K_{dr}, h, and the RMP. Values for K_{dr} are given on the x-axis, from the left panel to the right conduction of h is increasing, and the values for RMP are given different colors from blue (hyperpolarized) to red (depolarized). The dotted line gives the value for ADS and normalization of latency, respectively as observed in pain patients.

(Continued)

FIGURE 7 Continued
The black stars represent the optimal combination most similar to the values of ADS and normalization of latency in pain patients. Upper panel: the values for ADS for the model output with given parameter combinations. Lower panel: the values for normalization of latency for the model output with given parameter combinations. **(D)** Grid Search for the channel K_{dr}, the Na-K-pump, and the RMP. Values for K_{dr} are given on the x-axis, from the left panel to the right Na-K-pump rate is increasing, and the values for RMP are given in different colors from blue (hyperpolarized) to red (depolarized). The dotted line gives the value for ADS and normalization of latency, respectively as observed in pain patients. The black stars represent the optimal combination most similar to the values of ADS and normalization of latency in pain patients. Upper panel: the values for ADS for the model output with given parameter combinations. Lower panel: the values for normalization of latency for the model output with given parameter combinations.

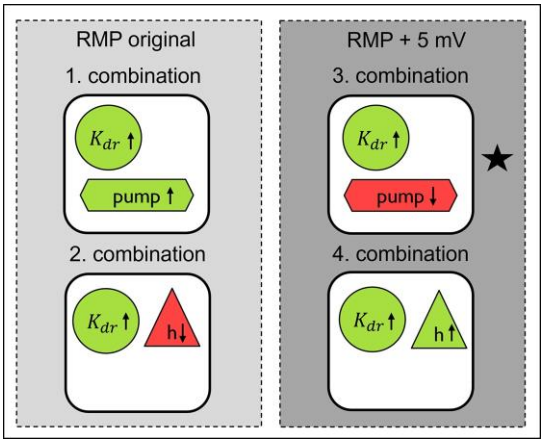

FIGURE 8
Best parameter combinations in computational model to simulate the changes observed in SFN patients with pain in comparison to healthy individuals and SFN patients without pain updated after grid search for original and depolarized RMP. Green indicates an increase in conductance or activity, while red indicates a decrease. The star indicates the combination which fits best to the pathological conditions previously observed in experimental work on neuropathy in human and in animal.

optimal value for Na-K-pump is in between the calculated values, which can be accepted due to the linear behavior of the simulated fiber in this scenario.

4.1.1 Summary of optimized parameter combinations

By conducting grid searches, we were able to optimize previously identified parameter values and identify mechanisms with low influence on ADS and normalization of latency, i.e., the conduction of the ion channels K_f and Na_v 1.7. Additionally, we discovered a previously unknown parameter set (increased Na-K-pump rate by 37.5% and an increased K_{dr} conduction by 50%). A schematic overview of the resulting parameter combinations is presented in Figure 8.

Executing the computational model with these parameter sets and a long axon of 10 cm, showed that the model performance had improved compared to previous results (Figures 4C,D). For three combinations ADS is near the original value, while simultaneously the normalization of latency is decreased sufficiently. For the last combination all parameter values were already optimal within the parameter space and could not be further improved. A figure showing the individual contributions of each ionic current during an action potential for the four final combinations can be reviewed in the Supplementary Figures (Figure A6).

4 Discussion

4.1 Model adaptations

In this study we employed a computational model to reproduce alterations in axonal propagation properties in C-fibers observed in small fiber neuropathy (SFN) patients with pain. We based our optimization on a large human data set derived from about 100 CM and CMi-fibers from SFN patients with and without pain and healthy controls. The computational model allows the observation and controlled manipulation of multiple parameters such as resting membrane potential (RMP), ion channel conductance and Na-K-pump rate. We were able to accurately replicate the observed changes and identified potential responsible mechanisms, shedding light on the underlying biological processes involved. For parameter optimization we applied a grid search method, where the model was executed 75 to 125 times per combination depending on the number of parameter changes. Therefore, the execution time of the model was crucial. We adjusted an existing nerve fiber model for C-fibers (Tigerholm et al., 2014) by reducing the length of the fiber from 10 cm to 1 cm and changing the morphology to a cylinder with uniform diameter and temperature. This led to a reduced computation time from over 1 h to just 7–10 min, which is crucial when considering the repetitive executions of 75 to 125 times in the grid search approach. We confirmed the fit of the model for CMi-fibers by comparing the result to microneurography data from healthy subjects and adjusted the diameter according to the best fit for the data. This validation with a large set of human data ensures a high quality of the computational model, which can be used to study potential ionic mechanisms underlying pain-related pathophysiological alterations in excitability.

4.2 Alterations in pain patients validated with previously unpublished data

In our previous publication with only a small patient number we found a more pronounced normalization of latency in pain patients in contrast to non-pain patients during lower stimulation frequency after a train of higher frequency stimulation (Kleggetveit et al., 2012). ADS can be seen as a self-inhibiting mechanism: more activity causes more ADS which is an indicator of hypoexcitability, because of accumulating sodium channel inactivation. Thus, a quicker normalization would indicate relative hyperexcitability for the amount

of previous activity and enable the fiber to discharge quicker following an AP and potentially producing more action potentials. Since ongoing pain in the feet is a typical and common symptom of SFN, it is hard to find SFN patients without ongoing pain in the feet and thus also the new group of patients without pain is small (Rasmussen et al., 2004). We thus added a large number of CMi-fibers from healthy volunteers. We compared the total ADS and the normalization of latency of SFN patients with and without pain with healthy volunteers. All groups showed no significant difference to each other in total ADS as observed before (Kleggetveit et al., 2012). Even though the difference between pain and non-pain patients was not significant, we observed that the course of the curve for non-pain patients and healthy subjects was very similar. Therefore, the non-significance could also be caused by the small sample size (9 non-pain patients) and a resulting higher standard error. This has to be investigated in further studies with larger sample sizes before we can draw definite conclusions. However, the normalization of latency of pain patients was significantly faster than for healthy subjects. While the magnitude of the difference (8.04%) might seem small, it remains a valid observation when compared with other parameters obtained in microneurographic recordings. While our results are not identical with the findings of Kleggetveit et al., they reflect the general trend that SFN patients with pain seem to have a faster recovery. Our results offer an explanation for the hyperexcitability and spontaneous activity in mechanoinsensitive C-nociceptors that are associated with spontaneous pain in peripheral neuropathy (Ochoa et al., 2005; Kleggetveit et al., 2012).

4.3 Individual mechanisms with largest impact on ADS and normalization

Via our model of a human C-fiber axon we set out to explore possible molecular mechanisms accounting for quicker normalization of latency, combined with unchanged ADS, a feature of CMi-fibers we observed in the SFN patients suffering from pain. We first varied single parameters individually. We found that changes in RMP and in the Na-K-pump rate have the greatest influence on both, ADS and normalization of latency. A reduction in Na-K-pump rate leads to an increase in ADS and a slower normalization of latency, which is an effect that can also be observed in elderly subjects (Namer et al., 2009). A reduction in Na-K-pump conductance would lead to accumulation of intracellular sodium (Tigerholm et al., 2014), which would result in increased ADS (De Col et al., 2008). Also, the potassium channel K_{dr} has a notable effect on ADS, i.e., a decrease in K_{dr} conduction leads to less ADS. It was proposed that the reduction of K_{dr} conduction could cause the membrane potential to repolarize slower after the peak of the action potential and therefore prevent recovery from slow inactivation of sodium channels (Petersson et al., 2014). This would lead to a reduction of sodium current in the subsequent action potential and ultimately less ADS (Petersson et al., 2014). Further, the hyperpolarization activated current h, which plays an important role during repetitive firing, largely affects the normalization. All variations of individual mechanisms have qualitatively the same effect on ADS as in Peterson et al., where a similar computational model was used with a different stimulation protocol to assess how variations in parameters affect the ADS (Petersson et al., 2014). The normalization of latency was not assessed there.

4.4 Combinations of multiple mechanisms reproducing stable ADS and faster normalization

In a nerve cell as well as in the computational model the conductance of different ion channels, the Na-K-pump rate and the RMP are all highly dependent on each other. Therefore, we investigated the interplay between these mechanisms and found several combinations which could replicate the effect of quicker normalization of latency as observed in SFN patients with pain. By adding the effects for ADS and normalization of latency for all possible combinations of variations of mechanisms, we discovered 18 candidates that could replicate the effect of faster normalization and stable ADS. We executed the model with these parameter combinations. We chose the best four combinations for further investigation and starting points in a grid search, since a grid search over all possible combinations would be too time consuming. This allowed us to optimize the parameter sets by finding the optimal value for each parameter and identifying parameters with low influence on the result, such as the conductance of the potassium channel K_f and the sodium channel Na_v 1.7. Additionally, via this grid search approach we discovered a previously unknown combination consisting of an increased Na-K-pump rate by 37.5% and an increased K_{dr} conduction by 50%. The grid search revealed further that the Na-K-pump and the hyperpolarization activated channel h have the opposite effect of each other, i.e., a reduction of the Na-K-pump rate leads to the same effect as an increase in conduction of h and vice versa. This is not surprising since the Na-K-pump drives sodium out of the cell and potassium into the cell, while h does the opposite. Nevertheless, the kinetics are vastly different, and activation of Ih occurs only at hyperpolarized potentials. The results suggest that Ih is active at RMP, especially, as we observed the opposite effect also on the RMP, which is an important mediator of the ADS and normalization. An increased Na-K-pump rate leads to a more hyperpolarized RMP, while an increase in conduction of h leads to a more depolarized RMP (Zhang et al., 2017). We found that the Na-K-pump and h are responsible for the faster normalization, but simultaneously decrease ADS. Therefore, the channel K_{dr} is needed to increase the ADS and bring it back to its original value. The combination of the mechanisms then leads to a stable ADS, while having a faster normalization. Interestingly, a depolarization of the RMP leads to the need for the Na-K-pump rate and the conduction of h to be adjusted in different directions to achieve the same effect, i.e., for a depolarized RMP the Na-K-pump rate needs to be reduced, while for the original RMP the Na-K-pump rate needs to be increased. The depolarization of the RMP leads to a much faster normalization of latency and less ADS, which is balanced out by increasing the conduction of h or decreasing the Na-K-pump rate.

Further, we elucidated via the grid search the interplay between different mechanisms. Especially, modulation of the Na-K-pump rate influenced the impact of other mechanisms on the result. A reduction of Na-K-pump rate causes the RMP and K_{dr} conduction to have a larger impact on the result, i.e., smaller changes in the RMP and K_{dr} conduction create larger differences in ADS. This shows that the interplay between different mechanisms is complex and hard to assess experimentally and therefore an investigation with computational models is helpful.

4.5 Physiological and clinical relevance

We set out to examine the influence of voltage gated sodium channels on the faster normalization of latency after a train of action potentials with a higher frequency as the importance of sodium channels for hyperexcitability of nociceptors in painful neuropathies has been shown in many studies (Cox et al., 2006; Fertleman et al., 2006; Goldberg et al., 2007; Huang et al., 2013; Brouwer et al., 2014). Additionally ADS is strongly influenced by sodium channel inactivation and intracellular sodium accumulation and associated with excitability of the neuron (De Col et al., 2008; Tigerholm et al., 2014). The slower a neuron conducts due to previous activity the less excitable it gets due to sodium channel inactivation and intracellular sodium accumulation. Therefore, ADS can be seen as self-inhibiting mechanism which protects from dangerous hyperactivity. Thus, when after certain activity the neuron returns quicker to its original conduction, the excitability necessary for producing action potentials again is reached quicker and higher discharge rates are possible. Interestingly, normalization turned out in our model to be modulated by different mechanisms than ADS, namely RMP, Na-K-pump, h and K_{dr} . Although this is still under debate, there are indications that the RMP could be depolarized in diabetic neuropathy (Krishnan and Kiernan, 2005). Additionally, patients with diabetic neuropathy show a reduced Na-K-pump function (Krishnan et al., 2008). Some peripheral neuropathies can be caused by mitochondrial disorders (Pareyson et al., 2013; Lee et al., 2020), which lead to a loss of energy in the cell and this could cause a reduced Na-K-pump rate. Taking those previous findings into account, the combination in Figure 8, which is marked with a black star, is the most likely to be present in patients. In our model in this specific combination of mechanisms the RMP is depolarized, the Na-K-pump rate is decreased and the channel conductance K_{dr} is increased. The reduced function of some K_{dr} channels leads to less mechanical and heat pain (Tsantoulas and McMahon, 2014). Here, we speculate that the opposite might also be true, i.e., an increase in conduction of K_{dr} might be associated to more pain via the above discussed mechanisms. Our model showed that in other combinations of mechanisms the hyperpolarization activated current h played a significant role. In rodent models blocking this channel leads to reduced discharge frequencies and reduced pain behavior (Chaplan et al., 2003; Jiang et al., 2008; Bernal and Roza, 2018), as well as decreases mechanical hyperalgesia (Luo et al., 2007; Young et al., 2014; Tsantoulas et al., 2017). Conversely, there are also studies which suggest the opposite, namely that blocking of h channels increases neuronal firing (Doan et al., 2004), which might lead to more pain. In the latter study the RMP was hyperpolarized, which could be an indication that the differences in these studies could be explained by different RMPs and point out the important role RMP plays. In Figure 8 we can observe that changes in the RMP lead to the need to adjust conduction of h in the opposite direction to achieve the same effect, i.e., for a depolarized RMP the conductance of h needs to be increased while for the original RMP the conductance of h needs to be decreased.

RMP alterations seem crucial to determine which mechanisms in the end are responsible for hyperexcitability in patient's nociceptors so that an individual variability in mechanisms leading to nociceptor hyperexcitability exists which calls for stratified or even personalized medicine in the treatment of neuropathic ongoing pain. It may also be possible that the mechanisms may not always be identical, and that several changes lead to similar results. This is underlined by the identification of several sets of parameters which are able to induce similar outcomes.

Mechanistically, a moderately depolarized membrane potential can be associated with hyperexcitability of nociceptors: A reduced rate of the Na-K-pump, as identified here in our simulations, supports depolarization. Depolarization leads to an increased fraction of inactivated sodium channels resulting in hypoexcitability, while at the same time it moves membrane voltage closer to the Na_v activation threshold, supporting hyperexcitability. However, it is unclear which mechanism predominates in determining excitability. Increased conductance of K_{dr} channels might lead to quicker and/or stronger repolarization following an action potential resulting in a higher fraction of available sodium channels supporting excitability. Thus, the identified mechanisms can contribute to hyperexcitability, and offer a potential peripheral mechanism of ongoing pain in some SFN patients with neuropathic pain.

Although significant differences in morphology and ion channel subtype composition are found in central nervous system (CNS) neurons and other experimental model neurons like in invertebrates, they show similar activity dependent changes of the nerve fiber conduction as unmyelinated peripheral primary nociceptive afferents (Zhang et al., 2017; Roth and Hu, 2020). Even if displayed in each study differently, ADS can be found in axons of CNS neurons and even in crustacean stomatogastric neurons (Zhang et al., 2017). In those publications, h, resting membrane potential and Na-K-pump is assumed to have major influence on activity-dependent modulation of axonal action potential conduction (Zhang et al., 2017; Roth and Hu, 2020). Thus, the contributions of Na-K-pump and h seem to be general peripheral and central axonal and evolutionary conserved mechanisms regulating the short-term memory of axons. Additionally, it was demonstrated in rodents that h and Na-K-pump both play an important role in the regulation of the resting membrane potential (Kim et al., 2007; Roth and Hu, 2020). Specifically, h depolarizes the RMP, while Na-K-pump hyperpolarizes it, when fibers are stimulated by high-frequency trains of spikes (Kim et al., 2007; Roth and Hu, 2020). It is still unclear if this also accounts for low frequency stimulation of C-fibers activity-dependent slowing as shown in the current study.

4.6 Limitations

The computational modeling of nerve cells is a valuable tool for studying neuronal function and behavior. The interplay of ion channels and other mechanisms can be evaluated without further inventions in humans. However, a computational model will always differ from a real nerve fiber in some respects. To be able to perform the necessary computations for our study, we had to reduce the complexity of the model. This was achieved by simplifying the morphology of the model, i.e., reduce the length of the fiber and have a uniform diameter and temperature across the fiber. In a real nerve fiber, diameter and temperature vary along its length, with a thinner

and cooler peripheral part. Since we assessed only a very short fiber this change could be neglected.

In the newly assessed data, the difference between SFN patients with and without pain could only be shown indirectly by comparing both groups with healthy subjects, due to a small sample size of patients without pain, since most patients with SFN have pain in the extremities. Nevertheless, the difference between healthy subjects and SFN patients with pain is in a similar range. The normalization of latency was nearly identical in healthy volunteers and patients without pain suggesting that a larger sample size of patients without pain might have produced a significant difference between patients with and without pain in the feet.

4.7 Future study considerations

In the current paper, we assessed the effects of regular stimulation in different frequencies over the time course of minutes on following latency normalization. In spontaneous activity and after chemical stimulation of nerve fibers a bursting behavior is often observed, i.e., the fiber exhibits a pattern of activity characterized by a series of action potentials that occur in rapid succession, followed by a brief period of inactivity. Since different mechanisms could modulate the effect of these burst, exploring this phenomenon further could be a valuable direction for future research. For this purpose, we propose to use a protocol mimicking these irregular discharges in small trains of action potentials. This protocol can provide valuable insights into the short-term effects on normalization and could be used in future computational studies to investigate the mechanisms involved. Since normalization is thought to play a key role in chronic pain conditions, using this protocol in microneurography experiments in healthy volunteers and SFN patients with and without pain could further deepen the understanding in differences between these groups. Overall, investigating these mechanisms can improve our understanding of the pathophysiology of pain and lead to the development of new therapeutic strategies.

5 Conclusion

Our study assesses the complex interplay between various ion channels, sodium potassium pump and resting membrane potential (RMP) modulating the normalization of latency. Our findings confirm that the normalization of latency is an important marker identifying pathological function of CMi-fibers of SFN patients with and without pain and healthy subjects, even when ADS is unchanged. In the past the importance of sodium channels in neuropathic pain disorders was often highlighted and they are undoubtedly a human validated pain target, as humans lacking functional $Na_v1.7$ are pain free. In the present study, we have indications that RMP, the Na-K-pump, the potassium channel K_{dr} and the hyperpolarization-activated current h are important modulators of normalization of latency and contribute to the pathologically modified CMi-fibers of SFN patients with ongoing pain. Moreover, we demonstrated that changes in the RMP have a major influence on other mechanisms so that opposite changes in conductance, result in similar effects on CMi-fiber function. Overall, these findings offer new avenues for targeted therapeutic interventions and highlight the potential of computational models in medical research.

Data availability statement

The datasets presented in this article are not readily available because of ethical and privacy restrictions. Requests to access the datasets should be directed to BN, bnamer@ukaachen.de.

Ethics statement

The studies involving humans were approved by Ethics committees from Aachen (EK 141/19) and Erlangen (4361). The studies were conducted in accordance with the local legislation and institutional requirements. The participants provided their written informed consent to participate in this study.

Author contributions

AM: Formal analysis, Software, Visualization, Writing – original draft, Writing – review & editing. EK: Methodology, Supervision, Writing – review & editing. MD: Data curation, Writing – review & editing. PS: Methodology, Supervision, Writing – review & editing. AL: Methodology, Validation, Writing – review & editing. JT: Conceptualization, Methodology, Supervision, Writing – review & editing. BN: Conceptualization, Data curation, Methodology, Resources, Supervision, Writing – review & editing.

Funding

The author(s) declare financial support was received for the research, authorship, and/or publication of this article. AM ans AL are funded by the Deutsche Forschungsgemeinschaft (DFG, German Research Foundation) – 368482240/GRK2416. JT is supported by the Center for Neuroplasticity and Pain is supported by the Danish National Research Foundation (DNRF121). BN is supported by a grant from the Interdisciplinary Center for Clinical Research within the Faculty of Medicine at the RWTH Aachen University, DFG NA 9707/1. This work was funded by the Deutsche Forschungsgemeinschaft German Research Foundation LA 2740/3–1, 363055819/GRK2415 Mechanobiology of 3D epithelial tissues (ME3T). AL, BN and MD are supported by a grant from the Interdisciplinary Center for Clinical Research within the Faculty of Medicine at the RWTH Aachen University (IZKF TN1-1/IA 532001, IZKF TN1-1IA 532002, IZKF TN1-6/IA 532006, and IZKF TN1-9/IA 532009).

Acknowledgments

We would like to express our gratitude to the patients and healthy volunteers for participating in our research. We would like to thank Prof. Manuel Torrilhon for fruitful discussions in the very early stages of the project.

Conflict of interest

The authors declare that the research was conducted in the absence of any commercial or financial relationships that could be construed as a potential conflict of interest.

The author(s) declared that they were an editorial board member of Frontiers, at the time of submission. This had no impact on the peer review process and the final decision.

Publisher's note

Supplementary material

The Supplementary material for this article can be found online at: https://www.frontiersin.org/articles/10.3389/fncom.2023.1265958/full#supplementary-material

SUPPLEMENTARY FIGURE A1
Performed workflow to find optimal parameter combinations, which reproduce the changed normalization of latency for SFN patients with pain in comparison to non-pain patients and healthy individuals. The grey boxes contain the performed computational steps and the additional text explains the rationale behind each step and the results obtained from it.

SUPPLEMENTARY FIGURE A2
ADS and relative latency for different combinations of ion channels, pump and resting membrane potential (RMP): in the left panel the relative latency for the full protocol is shown for different combinations of mechanisms compared to the original (black); in the right panel the relative latency for the last 10 pulses of the protocol is shown. The latency is normalized to the highest value of the ADS, so that all models start at 100%.

SUPPLEMENTARY FIGURE A3
Grid Search for the channels K_{dr}, h, and K_f. Values for K_f are given on the x-axis, from the left panel to the right K_{dr} is increasing, and the increasing values for h are given in different colors from blue to red. The dotted line gives the desired value for ADS and normalization of latency, respectively. Upper panel: the values for ADS for the model output with given parameter combinations. Lower panel: the values for normalization of latency for the model output with given parameter combinations.

SUPPLEMENTARY FIGURE A4
Grid Search for the channel K_{dr}, the Na-K-pump and RMP. Values for RMP are given on the x-axis, from the left panel to the right K_{dr} is increasing, and the increasing values for the Na-K-pump are given in different colors from blue to red. The dotted line gives the desired value for ADS and normalization of latency, respectively. Upper panel: the values for ADS for the model output with given parameter combinations. Lower panel: the values for normalization of latency for the model output with given parameter combinations.

SUPPLEMENTARY FIGURE A5
Grid Search for the channel K_{dr}, the Na-K-pump and RMP. Values for K_{dr} are given on the x-axis, from the left panel to the right RMP is increasing, and the increasing values for the Na-K-pump are given in different colors from blue to red. The dotted line gives the desired value for ADS and normalization of latency, respectively. Upper panel: the values for ADS for the model output with given parameter combinations. Lower panel: the values for normalization of latency for the model output with given parameter combinations.

SUPPLEMENTARY FIGURE A6
The ionic currents during an action potential for the four final combinations of the grid search. The panels on the left show all ionic currents, the panels on the right only the small ionic currents.

SUPPLEMENTARY FIGURE A7
Spike shape of all performed model evaluations. For Grid Search A (for the channels K_{dr}, h, and K_f) and Grid Search B (for the channels K_{dr}, h, and Na_v 1.7) all spike shapes resemble qualitatively the original model, while for Grid Search C (for the channels K_{dr}, h, and the *RMP*) and Grid Search D (for the channel K_{dr}, the Na-K-pump, and the *RMP*) some spikes show strange behavior and were excluded from the further analysis.

References

Bennett, D. L., Clark, A. J., Huang, J., Waxman, S. G., and Dib-Hajj, S. D. (2019). The role of voltage-gated sodium channels in pain signaling. *Physiol. Rev.* 99, 1079–1151. doi: 10.1152/physrev.00052.2017

Bernal, L., and Roza, C. (2018). Hyperpolarization-activated channels shape temporal patterns of ectopic spontaneous discharge in C-nociceptors after peripheral nerve injury. *Eur. J. Pain* 22, 1377–1387. doi: 10.1002/ejp.1226

Brouwer, B. A., Merkies, I. S. J., Gerrits, M. M., Waxman, S. G., Hoeijmakers, J. G. J., and Faber, C. G. (2014). Painful neuropathies: the emerging role of sodium channelopathies. *J. Peripher. Nerv. Syst.* 19, 53–65. doi: 10.1111/jns5.12071

Burke, D., Kiernan, M. C., and Bostock, H. (2001). Excitability of human axons. *Clin. Neurophysiol.* 112, 1575–1585. doi: 10.1016/S1388-2457(01)00595-8

Busserolles, J., Tsantoulas, C., Eschalier, A., and López García, J. A. (2016). Potassium channels in neuropathic pain: advances, challenges, and emerging ideas. *Pain* 157, S7–S14. doi: 10.1097/j.pain.0000000000000368

Chan, A. C. Y., and Wilder-Smith, E. P. (2016). Small fiber neuropathy: getting bigger! *Muscle Nerve* 53, 671–682. doi: 10.1002/mus.25082

Chaplan, S. R., Guo, H.-Q., Lee, D. H., Luo, L., Liu, C., Kuei, C., et al. (2003). Neuronal hyperpolarization-activated pacemaker channels drive neuropathic pain. *J. Neurosci.* 23, 1169–1178. doi: 10.1523/JNEUROSCI.23-04-01169.2003

Colloca, L., Ludman, T., Bouhassira, D., Baron, R., Dickenson, A. H., Yarnitsky, D., et al. (2017). Neuropathic pain. *Nat. Rev. Dis. Primer* 3, 1–19. doi: 10.1038/nrdp.2017.2

Cox, J. J., Reimann, F., Nicholas, A. K., Thornton, G., Roberts, E., Springell, K., et al. (2006). An SCN9A channelopathy causes congenital inability to experience pain. *Nature* 444, 894–898. doi: 10.1038/nature05413

De Col, R., Messlinger, K., and Carr, R. W. (2008). Conduction velocity is regulated by sodium channel inactivation in unmyelinated axons innervating the rat cranial meninges. *J. Physiol.* 586, 1089–1103. doi: 10.1113/jphysiol.2007.145383

De Col, R., Messlinger, K., and Carr, R. W. (2012). Repetitive activity slows axonal conduction velocity and concomitantly increases mechanical activation threshold in single axons of the rat cranial dura. *J. Physiol.* 590, 725–736. doi: 10.1113/jphysiol.2011.220624

Doan, T. N., Stephans, K., Ramirez, A. N., Glazebrook, P. A., Andresen, M. C., and Kunze, D. L. (2004). Differential distribution and function of hyperpolarization-activated channels in sensory neurons and mechanosensitive fibers. *J. Neurosci.* 24, 3335–3343. doi: 10.1523/JNEUROSCI.5156-03.2004

Fertleman, C. R., Baker, M. D., Parker, K. A., Moffatt, S., Elmslie, F. V., Abrahamsen, B., et al. (2006). SCN9A mutations in paroxysmal extreme pain disorder: allelic variants underlie distinct channel defects and phenotypes. *Neuron* 52, 767–774. doi: 10.1016/j.neuron.2006.10.006

Goldberg, Y. P., MacFarlane, J., MacDonald, M. L., Thompson, J., Dube, M.-P., Mattice, M., et al. (2007). Loss-of-function mutations in the Nav1.7 gene underlie congenital indifference to pain in multiple human populations. *Clin. Genet.* 71, 311–319. doi: 10.1111/j.1399-0004.2007.00790.x

Goodwin, G., and McMahon, S. B. (2021). The physiological function of different voltage-gated sodium channels in pain. *Nat. Rev. Neurosci.* 22, 263–274. doi: 10.1038/s41583-021-00444-w

Habib, A. M., Wood, J. N., and Cox, J. J. (2015). Sodium channels and pain. *Handb. Exp. Pharmacol.* 227, 39–56. doi: 10.1007/978-3-662-46450-2_3

Hines, M. L., and Carnevale, N. T. (1997). The NEURON simulation environment. *Neural Comput.* 9, 1179–1209. doi: 10.1162/neco.1997.9.6.1179

Hines, M., Davison, A., and Muller, E. (2009). NEURON and Python. *Front. Neuroinform.* 3:1. doi: 10.3389/neuro.11.001.2009

Huang, J., Han, C., Estacion, M., Vasylyev, D., Hoeijmakers, J. G. J., Gerrits, M. M., et al. (2014). Gain-of-function mutations in sodium channel Na(v)1.9 in painful neuropathy. *Brain J. Neurol.* 137, 1627–1642. doi: 10.1093/brain/awu079

Huang, J., Yang, Y., Zhao, P., Gerrits, M. M., Hoeijmakers, J. G. J., Bekelaar, K., et al. (2013). Small-Fiber neuropathy Nav1.8 mutation shifts activation to hyperpolarized potentials and increases excitability of dorsal root ganglion neurons. *J. Neurosci.* 33, 14087–14097. doi: 10.1523/JNEUROSCI.2710-13.2013

Jiang, Y.-Q., Sun, Q., Tu, H.-Y., and Wan, Y. (2008). Characteristics of HCN channels and their participation in neuropathic pain. *Neurochem. Res.* 33, 1979–1989. doi: 10.1007/s11064-008-9717-6

Kim, J. H., Sizov, I., Dobretsov, M., and von Gersdorff, H. (2007). Presynaptic Ca2+ buffers control the strength of a fast post-tetanic hyperpolarization mediated by the alpha3 Na(+)/K(+)-ATPase. *Nat. Neurosci.* 10, 196–205. doi: 10.1038/nn1839

Kist, A., Sagafos, D., Rush, A., Neacsu, C., Eberhardt, E., Schmidt, R., et al. (2016). SCN10A mutation in a patient with erythromelalgia enhances C-Fiber activity dependent slowing. *PLoS One* 11:e0161789. doi: 10.1371/journal.pone.0161789

Kleggetveit, I. P., Namer, B., Schmidt, R., Helås, T., Rückel, M., Ørstavik, K., et al. (2012). High spontaneous activity of C-nociceptors in painful polyneuropathy. *Pain* 153, 2040–2047. doi: 10.1016/j.pain.2012.05.017

Körner, J., and Lampert, A. (2020). "5.09 - Sodium Channels☆" in *The Senses: A Comprehensive Reference (Second Edition)*. (Ed.) Fritzsch, B. (Oxford: Elsevier), 120–141.

Krishnan, A. V., and Kiernan, M. C. (2005). Altered nerve excitability properties in established diabetic neuropathy. *Brain* 128, 1178–1187. doi: 10.1093/brain/awh476

Krishnan, A. V., Lin, C. S.-Y., and Kiernan, M. C. (2008). Activity-dependent excitability changes suggest Na^+/K^+ pump dysfunction in diabetic neuropathy. *Brain* 131, 1209–1216. doi: 10.1093/brain/awn052

Lee, S., Hoeijmakers, J. G. J., Faber, C. G., Merkies, I. S. J., Lauria, G., and Waxman, S. G. (2020). The small fiber neuropathy NaV1.7 I228M mutation: impaired neurite integrity via bioenergetic and mitotoxic mechanisms, and protection by dexpramipexole. *APSselect* 123, 645–657. doi: 10.1152/jn.00360.2019@apsselect.2020.7.issue-2

Luo, L., Chang, L., Brown, S. M., Ao, H., Lee, D. H., Higuera, E. S., et al. (2007). Role of peripheral hyperpolarization-activated cyclic nucleotide-modulated channel pacemaker channels in acute and chronic pain models in the rat. *Neuroscience* 144, 1477–1485. doi: 10.1016/j.neuroscience.2006.10.048

Maxion, A. (2023). Digital-C-Fiber/NEURON-C-fiber.

Namer, B., Barta, B., Ørstavik, K., Schmidt, R., Carr, R., Schmelz, M., et al. (2009). Microneurographic assessment of C-fibre function in aged healthy subjects. *J. Physiol.* 587, 419–428. doi: 10.1113/jphysiol.2008.162941

Namer, B., Ørstavik, K., Schmidt, R., Kleggetveit, I.-P., Weidner, C., Mørk, C., et al. (2015). Specific changes in conduction velocity recovery cycles of single nociceptors in a patient with erythromelalgia with the I848T gain-of-function mutation of Nav1.7. *Pain* 156, 1637–1646. doi: 10.1097/j.pain.0000000000000229

Ochoa, J. L., Campero, M., Serra, J., and Bostock, H. (2005). Hyperexcitable polymodal and insensitive nociceptors in painful human neuropathy. *Muscle Nerve* 32, 459–472. doi: 10.1002/mus.20367

Pareyson, D., Piscosquito, G., Moroni, I., Salsano, E., and Zeviani, M. (2013). Peripheral neuropathy in mitochondrial disorders. *Lancet Neurol.* 12, 1011–1024. doi: 10.1016/S1474-4422(13)70158-3

Pelot, N. A., Catherall, D. C., Thio, B. J., Titus, N. D., Liang, E. D., Henriquez, C. S., et al. (2021). Excitation properties of computational models of unmyelinated peripheral axons. *J. Neurophysiol.* 125, 86–104. doi: 10.1152/jn.00315.2020

Petersson, M. E., Obreja, O., Lampert, A., Carr, R. W., Schmelz, M., and Fransén, E. (2014). Differential axonal conduction patterns of mechano-sensitive and mechano-insensitive nociceptors – a combined experimental and modelling study. *PLoS One* 9:e103556. doi: 10.1371/journal.pone.0103556

Petroianu, G. A., Aloum, L., and Adem, A. (2023). Neuropathic pain: mechanisms and therapeutic strategies. *Front. Cell Dev. Biol.* 11:1072629. doi: 10.3389/fcell.2023.1072629

Prato, V., Taberner, F. J., Hockley, J. R. F., Callejo, G., Arcourt, A., Tazir, B., et al. (2017). Functional and molecular characterization of mechanoinsensitive "silent" nociceptors. *Cell Rep.* 21, 3102–3115. doi: 10.1016/j.celrep.2017.11.066

Rasmussen, P. V., Sindrup, S. H., Jensen, T. S., and Bach, F. W. (2004). Symptoms and signs in patients with suspected neuropathic pain. *Pain* 110, 461–469. doi: 10.1016/j.pain.2004.04.034

Roth, F. C., and Hu, H. (2020). An axon-specific expression of HCN channels catalyzes fast action potential signaling in GABAergic interneurons. *Nat. Commun.* 11:2248. doi: 10.1038/s41467-020-15791-y

Schmelz, M., Forster, C., Schmidt, R., Ringkamp, M., Handwerker, H. O., and Torebjörk, H. E. (1995). Delayed responses to electrical stimuli reflect C-fiber responsiveness in human microneurography. *Exp. Brain Res.* 104, 331–336. doi: 10.1007/BF00242018

Schmidt, R., Schmelz, M., Forster, C., Ringkamp, M., Torebjörk, E., and Handwerker, H. (1995). Novel classes of responsive and unresponsive C nociceptors in human skin. *J. Neurosci.* 15, 333–341. doi: 10.1523/JNEUROSCI.15-01-00333.1995

Sène, D. (2018). Small fiber neuropathy: diagnosis, causes, and treatment. *Joint Bone Spine* 85, 553–559. doi: 10.1016/j.jbspin.2017.11.002

Serra, J., Solà, R., Aleu, J., Quiles, C., Navarro, X., and Bostock, H. (2011). Double and triple spikes in C-nociceptors in neuropathic pain states: an additional peripheral mechanism of hyperalgesia. *Pain* 152, 343–353. doi: 10.1016/j.pain.2010.10.039

Strand, N., Wie, C., Peck, J., Maita, M., Singh, N., Dumbroff, J., et al. (2022). Small fiber neuropathy. *Curr. Pain Headache Rep.* 26, 429–438. doi: 10.1007/s11916-022-01044-8

Tigerholm, J., Petersson, M. E., Obreja, O., Eberhardt, E., Namer, B., Weidner, C., et al. (2015). C-Fiber recovery cycle Supernormality depends on ion concentration and Ion Channel permeability. *Biophys. J.* 108, 1057–1071. doi: 10.1016/j.bpj.2014.12.034

Tigerholm, J., Petersson, M. E., Obreja, O., Lampert, A., Carr, R., Schmelz, M., et al. (2014). Modeling activity-dependent changes of axonal spike conduction in primary afferent C-nociceptors. *J. Neurophysiol.* 111, 1721–1735. doi: 10.1152/jn.00777.2012

Torebjörk, H. E., and Hallin, R. G. (1974). Identification of afferent C units in intact human skin nerves. *Brain Res.* 67, 387–403. doi: 10.1016/0006-8993(74)90489-2

Tsantoulas, C., Laínez, S., Wong, S., Mehta, I., Vilar, B., and McNaughton, P. A. (2017). Hyperpolarization-activated cyclic nucleotide-gated 2 (HCN2) ion channels drive pain in mouse models of diabetic neuropathy. *Sci. Transl. Med.* 9:eaam6072. doi: 10.1126/scitranslmed.aam6072

Tsantoulas, C., and McMahon, S. B. (2014). Opening paths to novel analgesics: the role of potassium channels in chronic pain. *Trends Neurosci.* 37, 146–158. doi: 10.1016/j.tins.2013.12.002

Weidner, C., Schmelz, M., Schmidt, R., Hansson, B., Handwerker, H. O., and Torebjörk, H. E. (1999). Functional attributes discriminating mechano-insensitive and mechano-responsive C nociceptors in human skin. *J. Neurosci.* 19, 10184–10190. doi: 10.1523/JNEUROSCI.19-22-10184.1999

Young, G. T., Emery, E. C., Mooney, E. R., Tsantoulas, C., and McNaughton, P. A. (2014). Inflammatory and neuropathic pain are rapidly suppressed by peripheral block of hyperpolarisation-activated cyclic nucleotide-gated ion channels. *Pain* 155, 1708–1719. doi: 10.1016/j.pain.2014.05.021

Zhang, Y., Bucher, D., and Nadim, F. (2017). Ionic mechanisms underlying history-dependence of conduction delay in an unmyelinated axon. *elife* 6:e25382. doi: 10.7554/eLife.25382

Supplementary Material

Figure 1

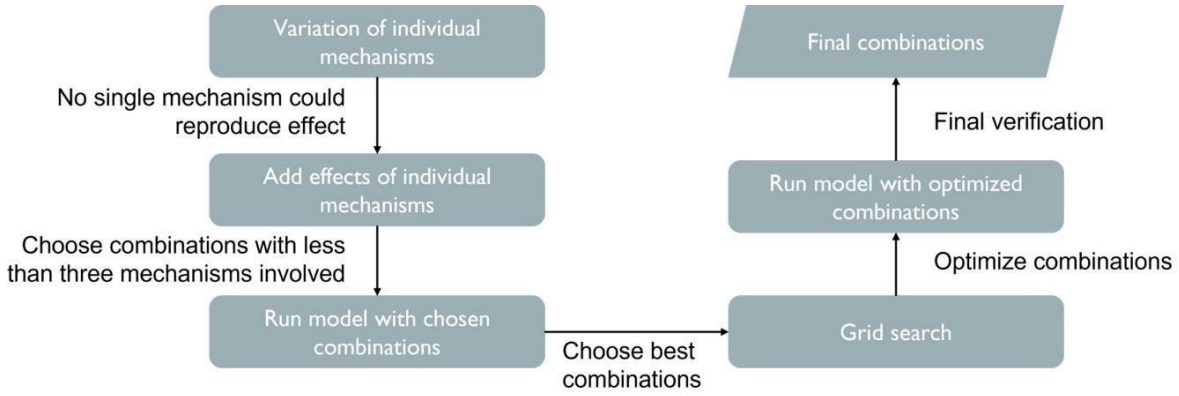

Figure 2

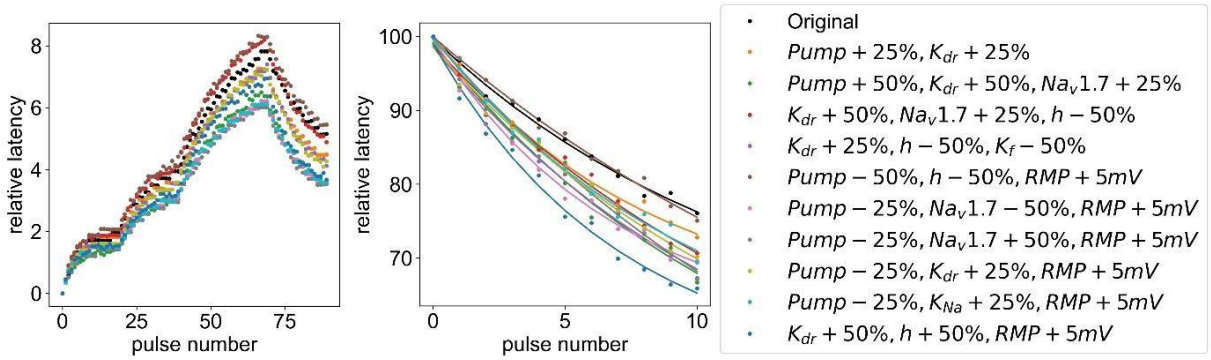

Figure 3

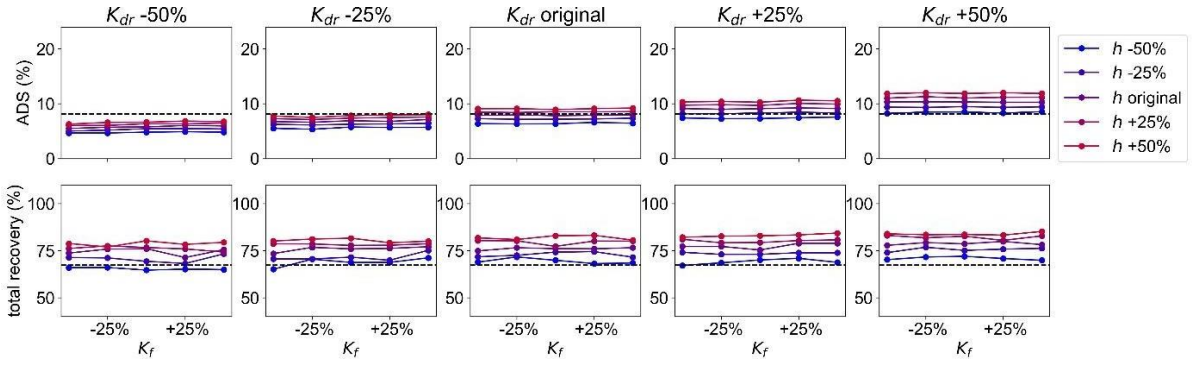

Figure 4

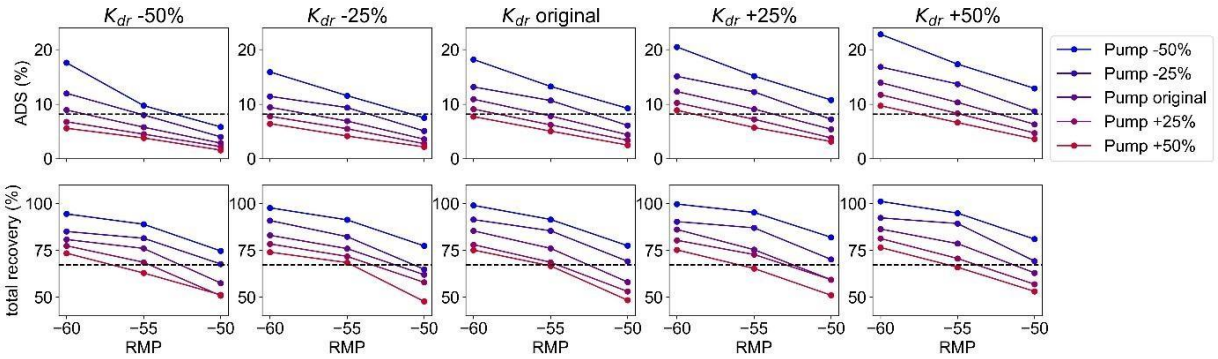

Figure 5

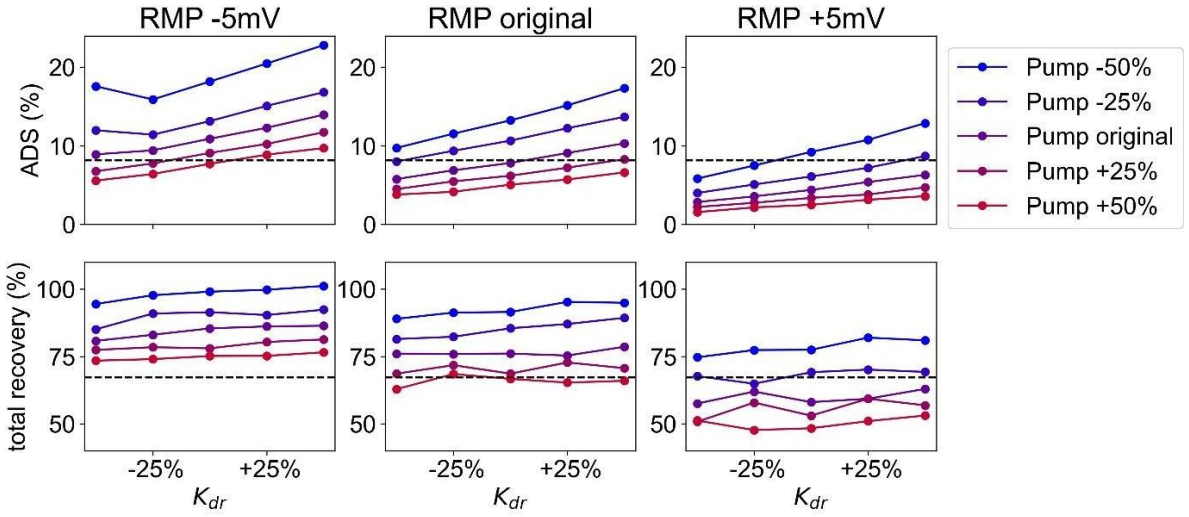

Figure 6

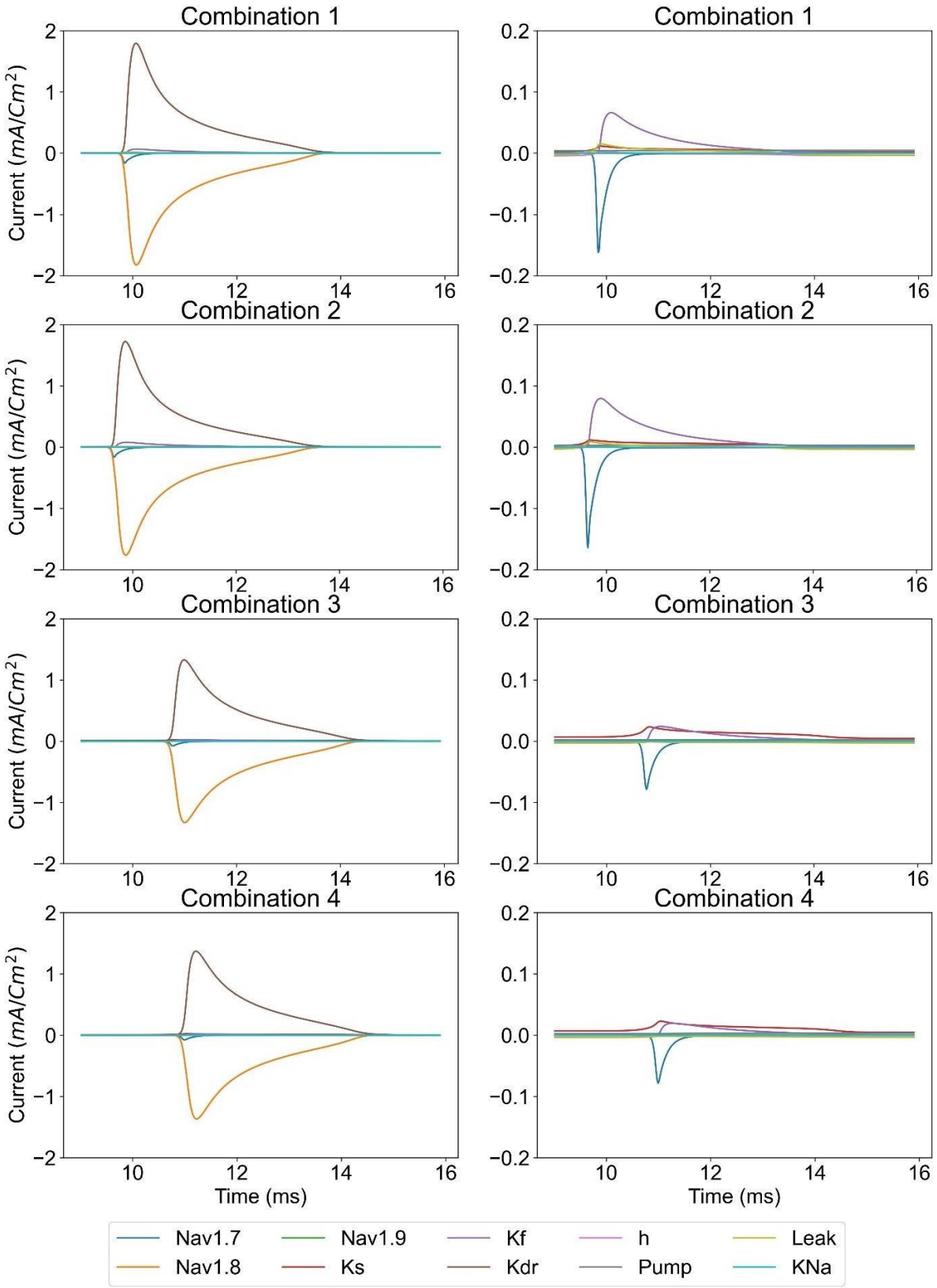
Combination 1
Combination 1
Combination 2
Combination 2
Combination 3
Combination 3
Combination 4
Combination 4
Current (mA/Cm²)
Time (ms)
Nav1.7
Nav1.8
Nav1.9
Ks
Kf
Kdr
h
Pump
Leak
KNa

Figure 7

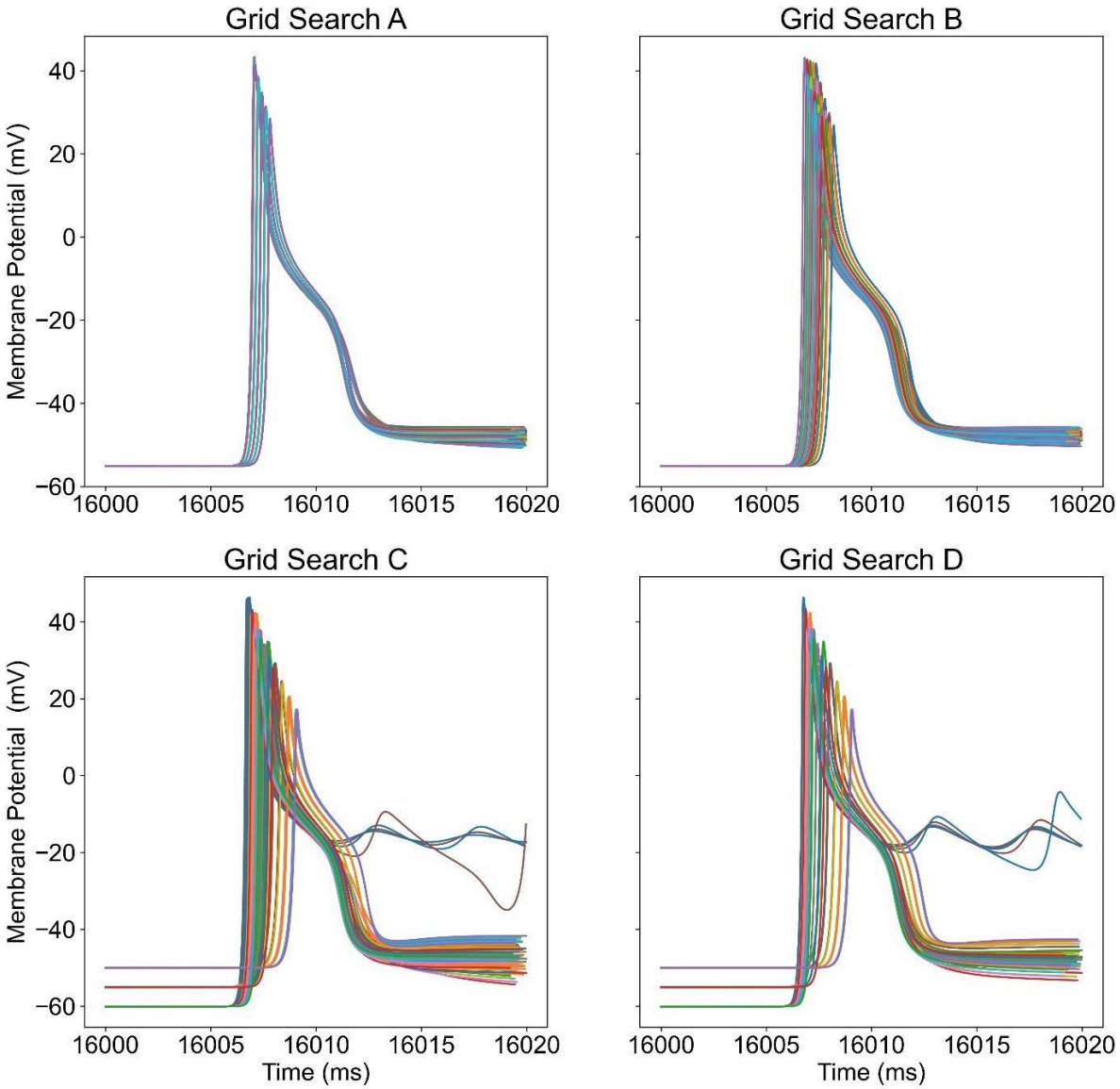
Grid Search A
Grid Search B
Grid Search C
Grid Search D
Membrane Potential (mV)
Time (ms)
40
20
0
−20
−40
−60
16000
16005
16010
16015
16020

Computer Methods and Programs in Biomedicine 255 (2024) 108319

Contents lists available at ScienceDirect

Computer Methods and Programs in Biomedicine

journal homepage: www.sciencedirect.com/journal/computer-methods-and-programs-in-biomedicine

Spectral changes in electroencephalography linked to neuroactive medications: A computational pipeline for data mining and analysis

Anna Maxion [a,*], Arnim Johannes Gaebler [b,c], Rainer Röhrig [d], Klaus Mathiak [b], Jana Zweerings [b], Ekaterina Kutafina [d,e]

[a] Research Group Neuroscience, Interdisciplinary Center for Clinical Research Within the Faculty of Medicine, RWTH Aachen University, Aachen, Germany
[b] Department of Psychiatry, Psychotherapy and Psychosomatics, Medical Faculty, RWTH Aachen University, Aachen, Germany
[c] Institute of Physiology, Medical Faculty, RWTH Aachen University, Aachen, Germany
[d] Institute of Medical Informatics, Medical Faculty, RWTH Aachen University, Aachen, Germany
[e] Institute for Biomedical Informatics, Faculty of Medicine, University Hospital Cologne, University of Cologne, Cologne, Germany

ARTICLE INFO

Keywords:
EEG
Electroencephalography
Open science
Reusable data
Computational psychiatry
Antipsychotics
Antiseizure
Drug-induced slowings
Epilepsy

ABSTRACT

Background and objectives: The increasing amount of open-access medical data provides new opportunities to gain clinically relevant information without recruiting new patients. We developed an open-source computational pipeline, that utilizes the publicly available electroencephalographic (EEG) data of the Temple University Hospital to identify EEG profiles associated with the usage of neuroactive medications. It facilitates access to the data and ensures consistency in data processing and analysis, thus reducing the risk of errors and creating comparable and reproducible results. Using this pipeline, we analyze the influence of common neuroactive medications on brain activity.

Methods: The pipeline is constructed using easily controlled modules. The user defines the medications of interest and comparison groups. The data is downloaded and preprocessed, spectral features are extracted, and statistical group comparison with visualization through a topographic EEG map is performed. The pipeline is adjustable to answer a variety of research questions. Here, the effects of carbamazepine and risperidone were statistically compared with control data and with other medications from the same classes (anticonvulsants and antipsychotics).

Results: The comparison between carbamazepine and the control group showed an increase in absolute and relative power for delta and theta, and a decrease in relative power for alpha, beta, and gamma. Compared to antiseizure medications, carbamazepine showed an increase in alpha and theta for absolute powers, and for relative powers an increase in alpha and theta, and a decrease in gamma and delta. Risperidone compared with the control group showed a decrease in absolute and relative power for alpha and beta and an increase in theta for relative power. Compared to antipsychotic medications, risperidone showed a decrease in delta for absolute powers. These results show good agreement with state-of-the-art research. The database allows to create large groups for many different medications. Additionally, it provides a collection of records labeled as “normal” after expert assessment, which is convenient for the creation of control groups.

Conclusions: The pipeline allows fast testing of different hypotheses regarding links between medications and EEG spectrum through ecological usage of readily available data. It can be utilized to make informed decisions about the design of new clinical studies.

Abbreviations: AD, antidepressant; AS, antiseizure; ASR, artifact subspace reconstruction; AP, antipsychotic; BDZ, benzodiazepine; EEG, electroencephalographic; FAIR, findable, accessible, interoperable and reusable; PET, positron emission tomography; SPECT, single photon emission tomography; TUH, Temple University Hospital.

* Corresponding author.
E-mail address: anna.maxion@rwth-aachen.de (A. Maxion).

https://doi.org/10.1016/j.cmpb.2024.108319
Received 14 November 2023; Received in revised form 2 July 2024; Accepted 5 July 2024
Available online 6 July 2024

1. Introduction

Neuroactive medications such as antidepressants, antipsychotics, or antiseizure medications exert their clinical effect by changing brain physiology. Most knowledge on the drugs' mechanisms of action has been gained by integrating findings from *in vitro* studies, *in vivo* animal research [1,2] as well as positron emission tomography (PET) [3–5] and single photon emission tomography (SPECT) [5,6] studies in human subjects.

However, nuclear medicine imaging studies using PET or SPECT are time-consuming and very demanding concerning both human and financial resources, thus effectively limiting the number of study participants. In comparison, electroencephalography (EEG) is a relatively affordable technique offering insights into brain dynamics with high temporal resolution. Indeed, several studies are using EEG data and its spectral properties as a proxy for assessing drug-related changes in patients' brains [7,8]. A recent perspective paper shows that functional biomarkers obtained from EEG measurements display potential for treating psychiatric disorders, even when the underlying pathophysiological processes are not fully understood [9]. Non-invasive biomarkers, such as EEG measurements, are of great interest for developing individualized treatment strategies since their appeal lies not only in their relevance to the targeted pathophysiology but also in the potential scalability and feasibility for clinical integration [10].

However, most available pharmaco-EEG studies typically have relatively low numbers of participants using single specific drugs. Furthermore, typically neither the raw data nor the computational code is made publicly available for reproducing the results or merging the data into a larger study. Big data analysis using large databases and standardized computational pipelines could hold the key to advancing our understanding of the impact of neuroactive medication on the brain and uncovering patterns and correlations that were previously elusive.

In the last years, the emerging concept of Open Science [11,12] and FAIR (Findable, Accessible, Interoperable and Reusable) [13–15] data handling led to the establishment of several databases [Physionet [16], HealthData.gov [17], Chronic Disease Data [18], World Health Organization [19]] with anonymized medical data, enabling the construction of comparable and reproducible computational methods. A world that is becoming more digitalized and thus creating more data every year is fueling this idea. A lot of this data remains still unused, which leads to a scientific and financial loss for society. Amongst other challenges, computational pipelines are needed to provide efficient data extraction and analysis approaches to facilitate utilization of the data and thus enable exploitation of the full potential of openly available data sets.

Temple University Hospital (TUH) EEG Corpus [20,21] with more than 30,000 data sets is currently the largest freely available database for research collection of medical EEG data. It provides both raw EEG signals and physicians' notes and is thus a source of valuable information. However, important challenges exist regarding the scientific use of the acquired data such as the efficient extraction of relevant information. In addition, physician's notes are semi-structured (i.e., imposing additional workload on data preparation), and sometimes incomplete (e.g., mostly no information on dosage of taken medications or psychiatric diagnosis), thus limiting the conclusions that can be drawn from the data. We want to address some of these challenges in the current manuscript.

Due to available human-labeled subsets, the TUH EEG Corpus was mainly used to develop and test machine-learning methods for the detection of epileptic seizures and EEG abnormalities [22–27]. By the time of manuscript submission, to our best knowledge, only Nahmias and colleagues [28] made use of the pharmaceutical data to develop a deep-learning approach to distinguish the users of two anticonvulsive medications based on their EEG data.

The current work aimed to develop a computational pipeline for mining and analyzing EEG data along with medication information from Temple University Hospital. The goal was to increase the accessibility of the TUH EEG Corpus to facilitate the conduction of research projects. As a demonstration of the utilization of the pipeline, we assessed drug-associated EEG spectral changes for antiseizure and antipsychotic drugs. The objective of this work is to support further research on the EEG changes linked to neuro-active medications by improving the accessibility of the database for physicians. We build an open-source computational pipeline that allows to mine TUH EEG Corpus for the records containing pre-defined medication names and preprocess the data by removing too-short records and standard artifacts. The spectral information is extracted for individual electrodes and compared for different groups of subjects. The calculated information is saved in Excel files. Finally, the results are visualized in topographic electrode maps. This pipeline allows the user to define their medication list of interest with further division into groups, and, depending on the research question, compare the spectral features of different drug users to each other. For advanced options, the open-source computational code can be adapted to adjust the pipeline to the medical research question, or to modify subsequent analytical steps by, e.g., using a different artifact detection procedure.

In this work, we will further assess the drug-associated EEG spectral changes and compare the output to findings in the literature on the example of two use cases for antiseizure and antipsychotic drugs. The results provide insights into the meaning and interpretability of the data and serve future users as a reference for selecting suitable options for the pipeline in the context of their respective research questions.

The built pipeline supports further research in the domain by providing an open-source mining tool that facilitates accessibility and utilization of the data to encourage more researchers to conduct projects with the provided data. It allows for well-controlled and reproducible results through the combination of open-source computational code and medical data.

2. Methods

2.1. Temple University Hospital database

For our project, we used the data from the Temple University Hospital (TUH) EEG Corpus [25], which contains over 30,000 anonymized EEG data files, collected since the year 2002 up to today. This database contains folders organized per patient. For one patient, multiple sessions and multiple files with EEG data can exist that are available in EDF format. In this format, not only can the raw binary signal data be stored, but also important metadata, such as the signal condition and the maximum amplitudes of the signal [20]. Additionally, physicians' reports are available in semi-structured text format. They include, among others, clinical history, a list of used medications, details of the EEG examination setup (electrodes, stimulation), evaluation of the EEG data, and clinical correlations, which describe the physicians' findings (see Fig. 1 for an example). Patients can have multiple medications listed in their report.

2.2. Ethical considerations

The data is openly available from [29] for any research purpose, after signing a data-sharing agreement. As stated in [30] and confirmed by the person responsible for the database, the study was conducted under the approval of the Temple University IRB (No 20,774) and the patients consent to the use of the anonymized data for research purposes.

2.3. Computational pipeline workflow

In the following, we will show the individual steps of our open-source processing pipeline [31]. The pipeline is written in MATLAB and uses the toolbox for signal processing of electrophysiological data EEGLAB [32]. A detailed overview of the full workflow is presented in Fig. 2.

HISTORY:
61 y.o. female with a history of ICH, venous thrombosis referred for routine
EEG. Currently with depakote prophylaxis, no history of seizures.
MEDICATIONS:
Xanax, percocet, depakote, coumadin
SEDATION: none
TECHNIQUE:
This is a technically challenging EEG. A Digital Video 21 channel electroencephalogram (EEG) was recorded using the International 10-20 system with T1/T2 electrodes and utilized a NicOne system. This EEG included a single channel of EKG and stimulation.
EEG BACKGROUND:
In wakefulness there is generous muscle artifact with an 11 Hz alpha rhythm intermittently disrupted on the left. There is also occasional bioccipital slowing noted.
During drowsiness, there is an increase in beta and slow rolling eye movements. In stage 1 sleep prominent POSTs are seen on the right only. In drowsiness there is also more rhythmic slowing from the left occipital region.
Sleep is characterized by vertex waves and spindles but are not sustained.
Mild generalized slowing is present.
Focal slowing is present.
EPILEPTIFORM ACTIVITY:
None
OTHER PAROXYSMAL ACTIVITY (NON-EPILEPTIFORM):
One burst of sharply contoured activity on the Left is noted
ACTIVATION PROCEDURES: Hyperventilation and photic stimulation are not performed.
EVENTS:
There are no clinical or electrographic events captured during this study.
HEART RATE:
A heart rate of max 90 bpm is captured on a single EKG lead but is slightly irregular.
IMPRESSION:
This is an abnormal awake and asleep routine EEG due to:
1. Background slowing and disorganization
2. Focal slowing on the left superimposed
3. Intermittent bioccipital slowing
CLINICAL CORRELATION:
The focal slowing is ipsilateral to the region of this patient's ICH. No definitive sharp waves were seen.

Fig. 1. Example of physicians' report with the sections "History", "Medications", "Sedation", "Technique", "EEG Background", "Epileptiform activity", "Other paroxysmal activity", "Activation procedures", "Events", "Heart rate", "Impression", "Clinical Correlation".

After deciding on the main study parameters, i.e., which individual drugs and which drug groups to include (drug list creation) and which comparisons to make, the pipeline handles the downloading and pre-processing of the data, the extraction of the spectral powers for each frequency band, statistical analysis and visualization of the data. Each step of the pipeline is modularized and can be adapted and run in consecutive steps.

Step 1. Drug list creation

The first modules in the pipeline require active decisions from the user to adjust the pipeline to the desired study design. The user creates a list of drugs and their trade names, classified according to their usage, for example, antidepressants, antipsychotics, etc. This can be easily done by creating a string array for each class with the names of the desired drugs that the class should contain. It is important to also add the trade names for each drug to the list since multiple names can be used in the physician's report for the same drug. For our use cases, we adapted a list of 28 drugs from Hyun [8] (see Table A1) and the trade names were obtained from the database drugs.com. The extensive list of common drugs of four different *classes* (antidepressant (AD), antipsychotic (AP), antiseizure (AS), and benzodiazepine (BDZ)) is already implemented in the pipeline and can be readily used.

Step 2. Choosing groups for comparison

In the next step, the user chooses the *comparison groups*, that can be defined as needed. Readily available options for comparison groups are the "Drug" group, which consists of all data files from patients that use one specific drug from the list, or the "Class" group, which contains any of the drugs in one class. In both cases, all files from patients who additionally take other drugs from the predefined list can be excluded (see next section "Data Mining"), which we will use as a standard in our use cases. A special comparison group is the "normal" class, which contains only EEG files labeled as "normal" and is explained in more detail in the next section. Each of these groups can now be compared with each other, i.e., possible comparisons are:

- Drug vs Drug,
- Drug vs Class,
- Drug vs "normal",
- Class vs Class,
- Class vs "normal".

The advantages and challenges of these comparison possibilities are discussed in the use cases.

Step 3. Data mining in TUH EEG Corpus

To search the TUH EEG Corpus fast and effectively, we cached the whole database into a table, which contains all files included in the TUH EEG Corpus with their corresponding file path, file type, last modified date, and a list of medications for each patient. This approach enabled us to search specifically for files from patients who used the pre-defined medications in Table A1. In the further processing of the data, it is possible to exclude patients who use more than one drug from the list, which we used as a standard in our use cases. Nevertheless, analyzing EEG profiles of individuals with multiple drug use is also in the scope of the pipeline. Additionally, all files labeled as "normal" in the TUH Abnormal Corpus [33] were saved.

To define a control data set, we used a subset of the EEG Corpus, namely TUH Abnormal Corpus (v2.0.0) [34]. This subset contains 3065

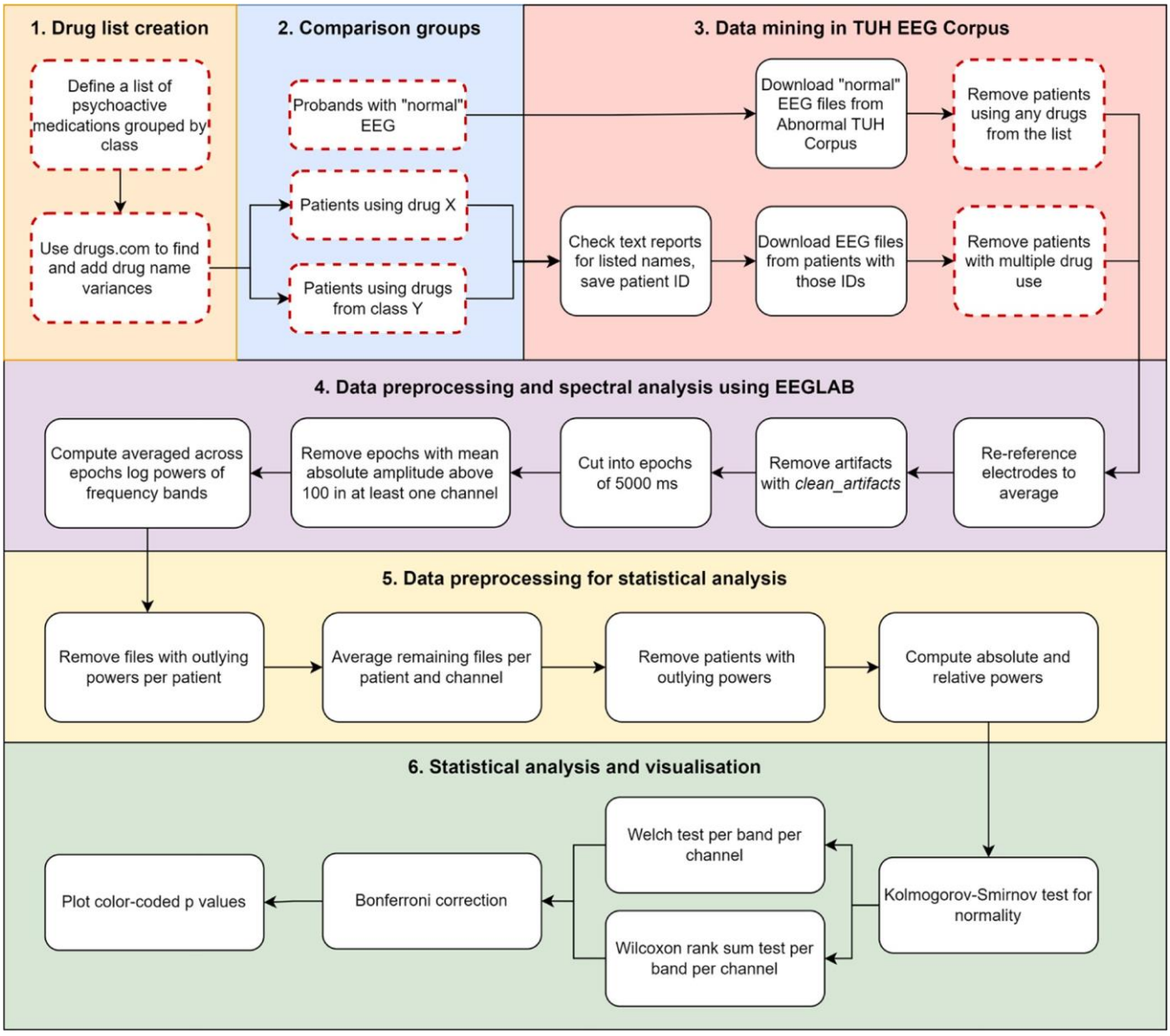

Fig. 2. Workflow of pipeline: Each module of the pipeline is shown in a different color. The squares with the red dashed lines mark steps in the process, where an active decision of the user is necessary.

EEG files, labeled as “normal” or “abnormal” for developing machine learning discriminative models. Each part of the database is further divided into “train” and “eval” parts. Here, we used all (train and evaluation) data labeled as “normal”, which resulted in 1521 files. From those, any files mentioning medications from the pre-defined list were removed, so that “normal” EEGs without the influence of drugs could be used as a reference.

Step 4. Data Preprocessing and Spectral Analysis using EEGLAB

The majority of data in the TUH Corpus employs the 10/20 system, a widely adopted arrangement of electrodes for EEG recordings, consisting of 21 evenly distributed scalp electrodes [35]. All files contain the following overlapping set of channels which are further used for the analysis: ’FP1′, ’FP2′, ’F3′, ’F4′, ’C3′, ’C4′, ’P3′, ’P4′, ’O1′, ’O2′, ’F7′, ’F8′, ’T3′, ’T4′, ’T5′, ’T6′, ’FZ’, ’CZ’, ’PZ’. Further, two common unipolar montages are used: the Average Reference (AR) and Linked Ears Reference (LE). The AR montage uses the average of specific electrodes as a reference, while the LE montage links the left and right ears for a stable reference point, aiming to reduce artifacts. During the preprocessing of the data, all files that used the LE reference method were re-referenced to AR.

For EEG preprocessing EEGLAB 2021.0 [32] was used in combination with MATLAB 2021a. EEG data was cleaned using the EEGLAB function *clean_artifacts,* which removes artifacts and tries to reconstruct the data via artifact subspace reconstruction (ASR). ASR is an automated, component-based method designed for removing transient, large-amplitude, or highly variable artifacts in multi-channel EEG recordings [36]. This technique identifies ’clean’ data segments automatically to serve as references and employs principal component analysis to eliminate artifacts in relation to the selected references. The underlying idea is that genuine brain signals, especially those concentrated in specific scalp regions, exhibit lower variation compared to artifacts. Consequently, artifacts become discernible in regions with minimized variance. Additionally, the function automatically detects and eliminates abnormal channels and segments of the data, such as short-term bursts. Channels are considered abnormal if they have a constant signal, a gradual frequency shift, have too much noise, or are not correlated to the other channels in the recording. The arguments used with this function were set to achieve a rather strict rejection of

artifacts. For each parameter of the function, a reasonable range for the values is given in the documentation of the function, ranging from "very aggressive" to "very lax". The fraction of channels that were allowed to contain artifacts that could not be removed in each time window was set to 0.05 (*WindowCriterion*), corresponding to a "very aggressive" parameter setting. A channel will be removed if it is of low quality for more than 15 % of the duration of the record (*ChannelCriterionMaxBadTime*), which aligns with a parameter setting that is considered to be "very aggressive". Portions of data that contained bursts were removed altogether (*BurstRejection*). All files where the function *clean_artifacts* returned an error were removed. Typically, the cause was the file being too short for the analysis (less than 3000 data points).

The data was further divided into epochs of 5000 ms. The choice of 5000 ms for epoch length was based on the studies [33,36,37,39,41] we used for comparisons with our results, which used epochs between 2.5 s and 30 s with a median of 4 s. The chosen epoch length balances the trade-off between capturing enough signal information within each epoch while also avoiding the risk of non-stationarity of EEG signals over time. Our analysis did not use overlapping epochs as it can introduce autocorrelation and increase computational complexity.

During the implementation and testing of the pipeline, we manually inspected portions of the data following the utilization of the *clean_artifacts* procedure to ensure the quality of the data. We identified the continued presence of artifacts exhibiting elevated amplitude levels, potentially attributable to ocular blinking, muscular activity, and related factors. Subsequently, we constructed the pipeline to eliminate these artifacts by automatically excluding epochs with mean absolute amplitude greater than 100 microvolts for at least one channel from further analysis. The affected epochs were removed across all channels.

EEGLAB function *spectopo* was used to compute averaged per channel powers of the frequency bands defined as follows (units in hertz): delta= [1, 3.5], theta= [3.5, 7.5], alpha= [7.5, 12.5], beta= [12.5, 30] and gamma = [30, 60].

Step 5. Data Preprocessing for Statistical Analysis

For each patient, file-wise outlier removal was performed by excluding all elements that exceeded three standard deviations from the mean. The remaining files were averaged to obtain a single number for each band and channel per patient. Finally, across-patient outliers were removed again by excluding all elements that exceeded three standard deviations from the mean. We also calculated the ratio alpha/theta in addition to the individual frequency bands. This value is used as a marker for diseases like Alzheimer's [37] and Parkinson's [38]. In addition to the calculated absolute powers, we computed relative powers by dividing the power spectrum of each patient for each band and channel by the sum of all band powers for the respective channel, see Formula (1).

$$relativePower_{band,\ channel} = \frac{power_{band,\ channel}}{\sum power_{band,\ channel_{band}}} \quad (1)$$

Step 6. Statistical Analysis and Visualization

For the chosen comparison groups, a one-sample Kolmogorov-Smirnov test is used to test each group for normality in each electrode and frequency band. In every electrode and frequency band where the test confirms the normal distribution of both groups, a *t*-test is used for comparison. To prevent issues with non-matching variances, we used Welch's two-sample *t*-test. In every electrode and frequency band where the normal distribution cannot be confirmed, a two-sided Wilcoxon rank sum test is performed. Additionally, a Bonferroni correction to prevent an accumulation of errors due to multiple testing of the same data set. Color-coded *P* values are plotted in an electrode plot for each frequency. Blue represents decreasing values compared to the reference group, while red represents increasing values.

2.4. Use cases: antiseizure carbamazepine and antipsychotic risperidone

To illustrate some of the possible outputs and usages of the pipeline the antiseizure drug carbamazepine and the antipsychotic drug risperidone were chosen. Both drugs are well-represented in the database and well-researched in the literature.

3. Results

Before downloading and processing the data, the whole database is cached into a table, to increase the speed of searching in the database. The process of caching requires approximately a week, but it is also possible to only cache parts of the database. The downloading time of the individual data files depends on the file size. For risperidone, all files were downloaded in approximately 3 h, which leads to an average downloading time of circa 315 files per hour. Downloading all data listed in Table A1 in the Appendix requires circa 120 h. The artifact cleaning of the data for risperidone required approximately 1 h 20 min, which leads to an average of 730 files/h and circa 52 h for all data used in this paper. During the cleaning of the data, all unusable files are removed, therefore the next steps of processing the data will be faster due to less data. Computing the power spectrum of the data requires approximately 5 min for 100 files, which leads to a calculation time of circa 15 min for risperidone and circa 29 h for all our data. The rest of the processing, statistical analysis, and visualization of the data is comparatively fast. Each comparison of the full drug groups only requires a couple of minutes.

From the general TUH EEG Corpus, we downloaded 37,746 files from 8871 patients, who had used drugs from the list in Table A1, where the exact number of files and patients for each drug is listed. After cleaning and artifact removal, as well as removal from outliers, there were 34,419 files from 8078 patients left. Demographics for patients were not extracted for the presented use cases due to inconsistent and missing data in patients' records. However, we are working on enhancing our pipeline to enable us to extract data more effectively from these records in future iterations.

The "Abnormal EEG Corpus" consists of reviewed data of good quality. Therefore, out of the original 1521 files, artifact cleaning did not remove any files. After excluding patients receiving any neuroactive drugs according to our keywords, 881 files from 840 patients remained. Finally, after the removal of the outliers, 632 patients were left.

3.1. Use case 1: antiseizure medication carbamazepine

To show an example of how the framework can be used we chose the well-researched drug carbamazepine. carbamazepine is an antiseizure medication and is mainly used for epilepsy, bipolar disorder, and neuropathic pain. The database contained 2865 files from patients taking carbamazepine. After artifact cleaning 2315 files from 348 patients remained, which left 276 patients for comparison after averaging individual files for each patient and outlier removal. We further removed all patients taking multiple drugs from the pre-defined list in Table A1 to eliminate drug interactions and to investigate the effect of only the specific drug in question. This left 173 patients in the carbamazepine group.

3.1.1. Drug vs. "normal"

We compared the carbamazepine group to the "normal" (i.e., control) dataset for each band and electrode separately using a multiple-test correction. The resulting *P* values for absolute and relative powers are visualized in Fig. 3. A power increase in relation to the control dataset is visualized by coloring the electrodes red, while a power decrease is indicated in blue.

For absolute powers, in the carbamazepine group, delta and theta bands were significantly higher as compared to the "normal" group. For the alpha and beta bands the central electrode "Cz" was increased and for gamma, no significant changes were detected.

For relative powers, alpha, beta, and gamma were decreased over the whole electrode map. Delta and theta both increased, while the increase

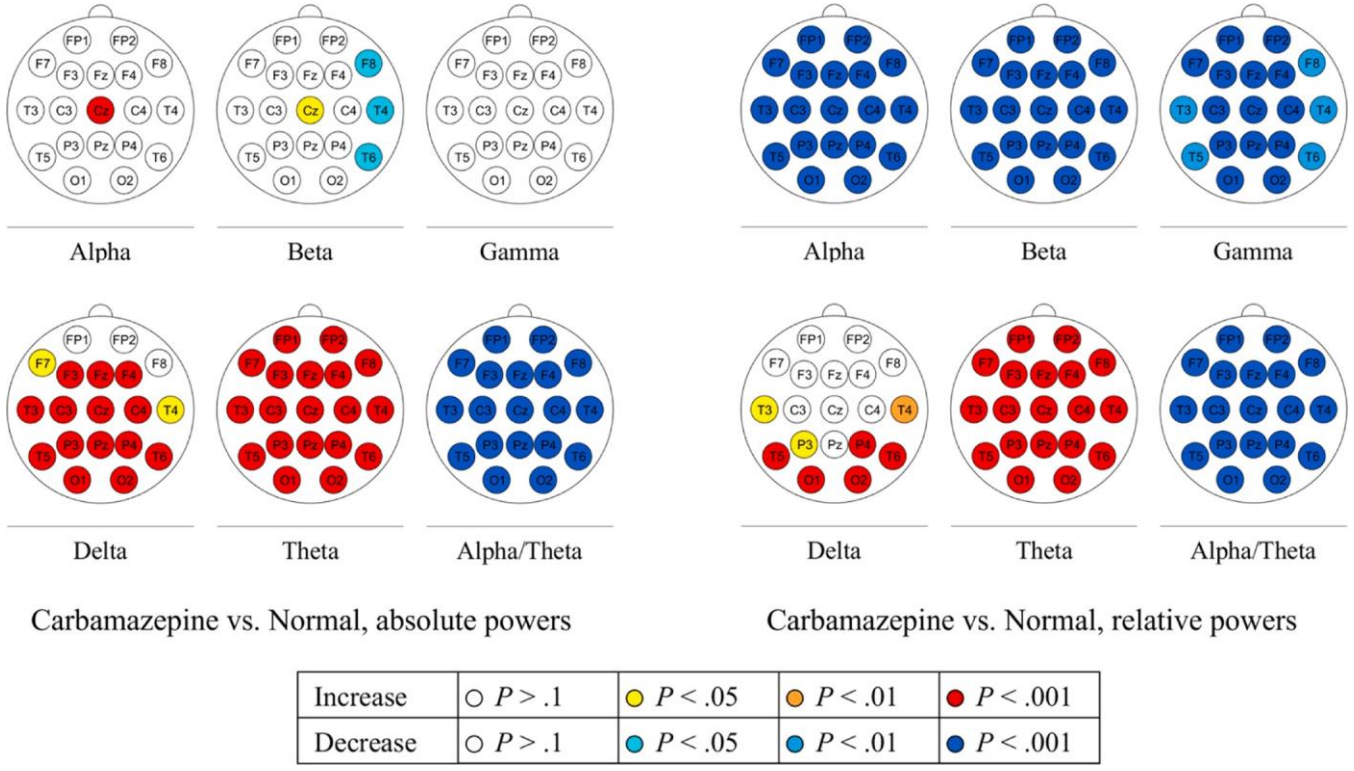

Fig. 3. P values from Welch's test for the carbamazepine group ($n = 173$) compared to the "normal" class ($n = 632$) per channel. Red and blue colors indicate power increase and decrease, respectively. In addition to the basic bands, the alpha/theta ratio is shown. Each set of tests is computed for absolute and relative powers. A Bonferroni correction for multiple testing is applied.

in delta was restricted to the posterior region of the electrode map. Alpha/theta decreased for absolute and relative powers in all leads.

3.1.2. Drug vs. class

The antiseizure class (AS) consists of the common drugs carbamazepine, valproate, lamotrigine, topiramate, and levetiracetam. These

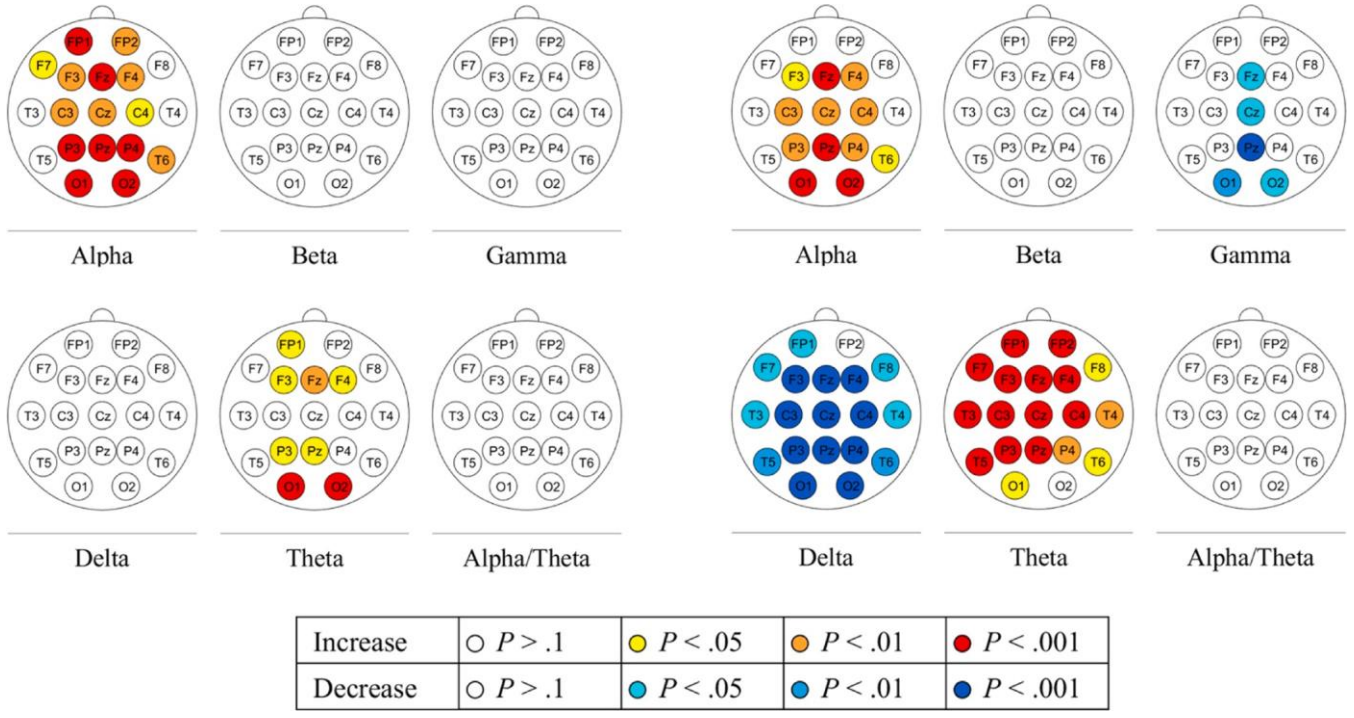

Fig. 4. P values from Welch's test for the carbamazepine group ($n = 173$) compared to the remaining drugs of the antiseizure class (AS) ($n = 3644$) per channel. Red and blue colors indicate power increase and decrease, respectively. In addition to the basic bands, the alpha/theta ratio is shown. Each set of tests is computed for absolute and relative powers. A Bonferroni correction for multiple testing is applied.

drugs were well represented in the database with more than 19,000 files altogether, compare with Table A1. After processing the data, 3644 patients remained in the class. Here we want to compare the drug carbamazepine with the remaining drugs in the class. The results for the comparison of carbamazepine with the antiseizure class are shown in Fig. 4.

For the absolute powers, an increase in alpha and theta frequency was observed. The relative powers increased in alpha and theta bands, while gamma and delta were decreased. Delta showed decreasing behavior over almost the whole electrode map, while gamma only decreased in a few electrodes. No change emerged for beta and the alpha/theta ratio, neither for absolute nor relative powers.

3.2. Use case 2: antipsychotic medication risperidone

As a second example, the antipsychotic drug risperidone was chosen, which is mainly used to treat schizophrenia and bipolar disorder. For this drug 946 files from 277 patients were found in the database. After artifact cleaning 392 files from 84 patients remained. When filtering out all patients who took multiple drugs on the list, 74 files from 58 patients were left, which was further reduced to 40 patients after averaging all files from each patient and removing outliers.

3.2.1. Drug vs. "normal"

When compared to the "normal" class, patients receiving risperidone, see Fig. 5, exhibited lower absolute and relative powers of alpha, beta, gamma, and alpha/theta. The relative power within the delta and theta band was increased, while the absolute power of delta was decreased on the right side of the scalp and the absolute power of theta showed no changes. The absolute powers of alpha, beta, and gamma, as well as the relative power of alpha, mainly decreased in the outer regions of the scalp. The relative power of beta decreased in all electrodes, while gamma was only decreased in "Cz". The increasing relative delta powers were focused on the occipital and parietal regions, while the increasing relative theta powers were spread additionally to temporal and central regions. Alpha/theta was decreased in all electrodes for relative and absolute powers.

3.2.2. Drug vs. class

We created an antipsychotic class (AP) consisting of risperidone, aripiprazole, haloperidol, olanzapine, quetiapine, and ziprasidone, see Table A1. It contains 2195 cleaned files from 806 patients.

When risperidone was compared to the remaining drugs in the AP class, see Fig. 6, a decrease in absolute power emerged in the delta band for occipital, parietal, right temporal, and the central electrode "C4". For all other bands and for all bands for relative powers, no significant change was observed.

4. Discussion

4.1. Computational pipeline performance

The presented MATLAB pipeline mines the TUH EEG Corpus and compares the spectral features between different groups of patients defined based on their medication profile. The key feature of the pipeline is flexibility. It can be changed to answer a variety of medical and technical research questions while standardizing necessary procedures, such as extraction and cleaning of the data. The list of medications and the defined comparison groups can be easily modified by researchers without computational background. The user chooses the drugs of interest, as well as their organization into classes. Subsequently, the user can choose between different possible comparisons: Drug vs Drug, Drug vs Class, Drug vs "normal", Class vs Class, or Class vs "normal". Thus, a wide range of possibilities exist, and the researcher must carefully consider which comparisons are adequate based on the individual study design and for comparisons to the existing literature. Different modules

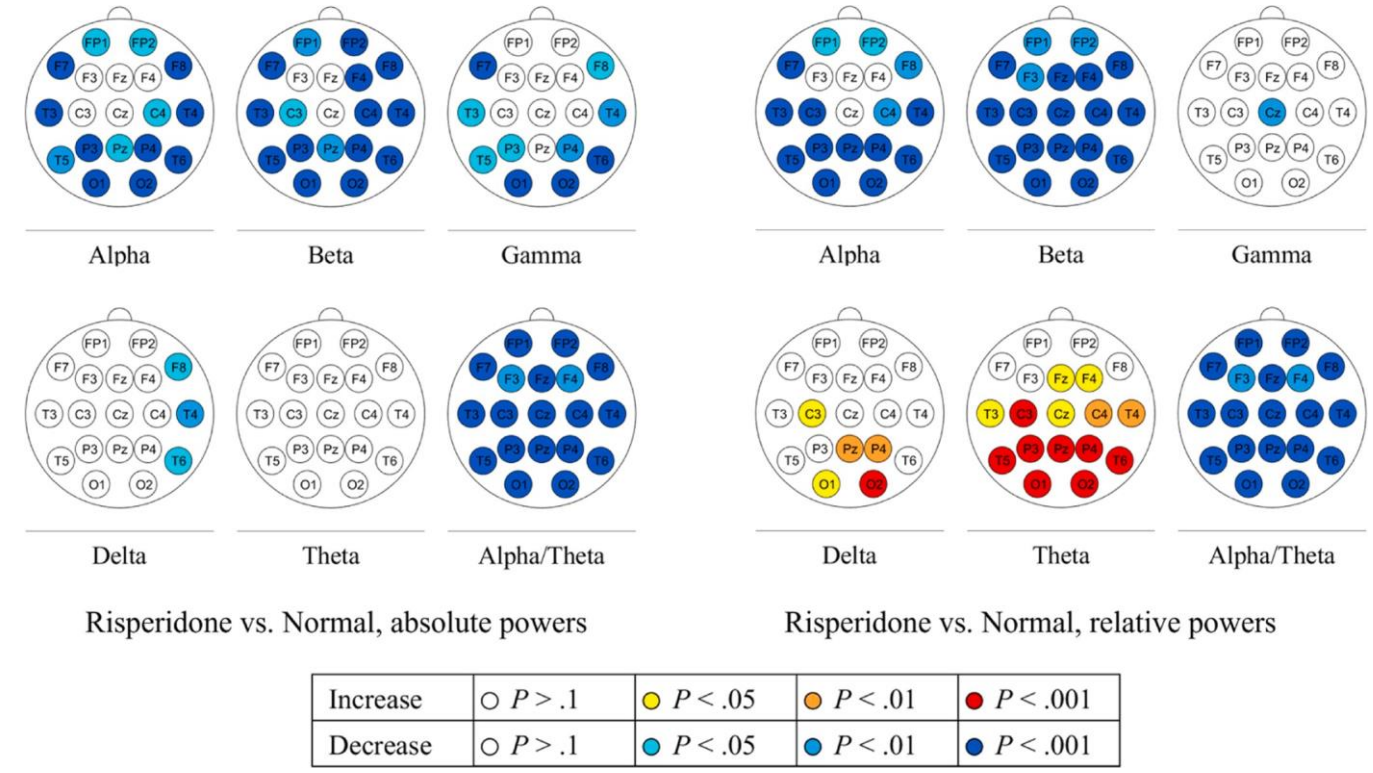

Fig. 5. P values from Welch's test for the risperidone group ($n = 40$) compared to the "normal" class ($n = 632$) per channel. Red and blue colors indicate power increase and decrease, respectively. In addition to the basic bands, the alpha/theta ratio is shown. Each set of tests is computed for absolute and relative powers. A Bonferroni correction for multiple testing is applied.

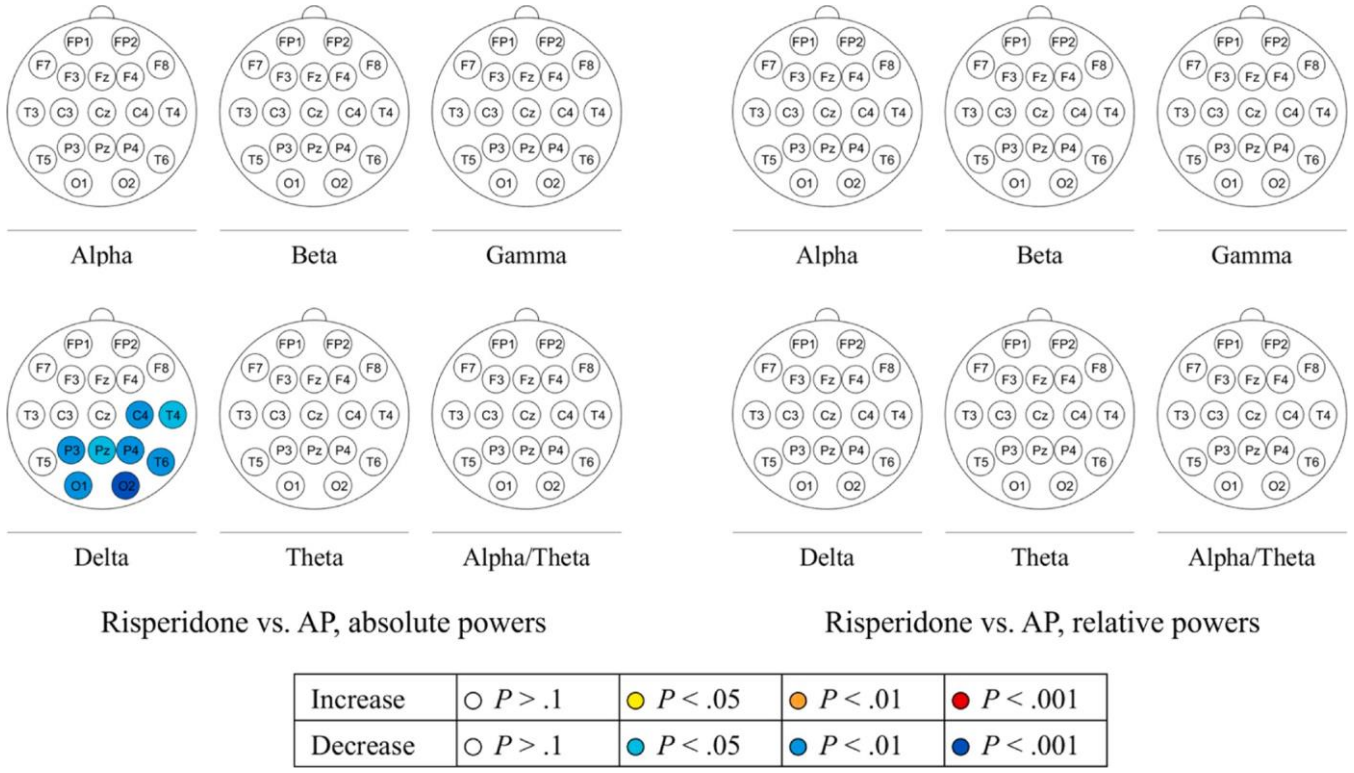

Fig. 6. P values from Welch's test for the risperidone group (n = 40) compared to the remaining drugs of the antipsychotic class (AP) (n = 806) per channel. Red and blue colors indicate power increase and decrease, respectively. In addition to the basic bands, the alpha/theta ratio is shown. Each set of tests is computed for absolute and relative powers. A Bonferroni correction for multiple testing is applied.

of the pipeline download, preprocess, and analyze the data, which allows good control of the analytical process.

Files that are classified as "normal" (i.e., the EEG signal is similar to the signal of a healthy person) can be treated as a control group. We can further track the drug intake of this group to create a control group with or without drug intake. For the drug groups, we can also control the drug intake of other drugs and therefore create a treatment group with or without multiple drug use.

The pipeline is restricted by the limitations of the TUH EEG Corpus. The metadata is only semi-structured and limited to standard clinical information, therefore full control of all potentially relevant study parameters is not possible.

The FAIR Guiding Principles, introduced to enhance the accessibility and usability of scholarly data, promote findability, accessibility, interoperability, and reusability by both humans and machines. Originally designed for data, the principles were intended to extend to digital objects like algorithms, tools, and workflows that contribute to data generation. An overview of the FAIR principles for software is given in [39].

Our work not only shows the significance of open-access medical data that adheres to these principles but also the importance of FAIR software. Therefore, our developed computational pipeline aligns with key aspects of FAIR software principles. We ensure the findability and accessibility by documenting comprehensive details about its purpose and functionalities in this manuscript. The software, along with its documentation, is made discoverable through inclusion in a searchable software registry, notably GitHub, providing a centralized location for users to locate and access the latest version. The interoperability is addressed as the software employs a widely used language (MATLAB), while the documentation uses text and word files. Reproducibility is a key focus, ensured by the documentation of the software and the detailed description of the pipeline in this manuscript, which includes detailed provenance information, i.e. documenting the origin and history of the data. The software documentation adheres to domain-relevant community standards, reinforcing the pipeline's commitment to the principles of FAIR software.

4.2. Medical insights

We compared our findings regarding the EEG changes of carbamazepine and risperidone compared to the "normal" group and the antiseizure and antipsychotic group, respectively, with existing literature to identify and discuss consistencies and discrepancies. We will discuss each drug separately followed by a general discussion on the comparability of the findings and the literature. An overview of our findings for absolute and relative powers is presented in Table 1.

When we consider carbamazepine vs. "normal", we observe an overall increase in delta and theta frequency bands for absolute and relative powers. The increase in delta is also observed by [40–43] and the increase in theta is observed by [41–44]. Further, we discovered a decrease in the relative powers of alpha and beta. The findings for alpha are in line with [40,41,43,44]. For beta, the information in the literature is inconclusive with either no change [44] or inconsistent changes [41] reported. Gamma is decreasing for relative powers and alpha/theta is consistently decreasing for absolute and relative powers. We found no information in the literature on the gamma frequency band or on the results for alpha/theta.

Even though the results in the literature are mostly consistent with the present findings, the methods of the studies differed. Marciani et al. [40], Besser et al. [41], Frost et al. [43] and Wu et al. [44] examined epileptic patients before and after treatment, but the time intervals for the EEG measurements differed largely, ranging from 2 h up to 2 months after the beginning of the treatment. Wu et al. [44] additionally examined healthy volunteers before and after treatment. Mecarelli et al. [42] also investigated healthy subjects. They compared the effects before vs. after treatment as well as treatment vs. placebo and treatment vs. other

Table 1
Overview of the changes in absolute and relative power spectrum induced by carbamazepine and risperidone compared to the normal group, the antiseizure group (AS), and the antipsychotic group (AP), respectively. The increase (+) / decrease (-) in the power spectrum is observed in at least one electrode. If no changes were observed, it is marked as 0. The numbers in the brackets are references to studies that observed similar effects.

Drug	Alpha	Beta	Gamma	Delta	Theta	Alpha /Theta	Absolute or relative power
Carbamazepine vs. Normal	+	+/-	0	+ [40–43]	+ [41–44]	–	absolute
Carbamazepine vs. Normal	- [40,41,43,44]	–	–	+ [40–43]	+ [41–44]	–	relative
Carbamazepine vs. AS	+ [42]	0	0	0	+ [42]	0	absolute
Carbamazepine vs. AS	+	0	–	–	+	0	relative
Risperidone vs. Normal	–	- [45]	–	–	0	–	absolute
Risperidone vs. Normal	–	–	–	+	+	–	relative
Risperidone vs. AP	0	0	–	0	0	0	absolute
Risperidone vs. AP	0	0	0	0	0	0	relative

drugs.

When we compare carbamazepine to the class of antiseizure drugs, we observe an increase in alpha and theta in the absolute powers. The delta frequency band shows no significant changes for absolute powers. Mecarelli et al. [42] reported a significant increase in the absolute powers of the delta frequency band when they compared carbamazepine with the antiseizure medications oxcarbazepine and levetiracetam in healthy volunteers. Values for alpha and theta bands were also increased, but those changes were not significant, which could be due to the small sample size of only 10 volunteers.

For the risperidone vs. "normal" comparison, we observe almost no changes in absolute powers of delta and theta and an increase in relative powers of delta and theta. Hughes et al. [46] reported an increase in absolute powers for delta and theta for closed eyes, while for open eyes, only theta was increased. Lee et al. [47] described the increase in absolute delta and theta in all electrodes. Mucci et al. [45] noted that fast theta was increased. All three mentioned studies reported these results for the short-term effects in the first 24 h. For the long-term effects after 6 weeks of treatment, Mucci et al. [45] reported a general increase in fast theta for all patients and a decrease in slow theta for patients who responded to the drugs, while non-responders showed the opposite behavior.

For alpha and beta, we observed a decrease. Lee et al. [47] observed no changes in alpha and beta, and Hughes et al. and Mucci et al. an increase in slow alpha and slow beta for short time effects. Mucci et al. also observed a decrease in fast beta. For long-term effects, the authors reported an increase in slow beta for all patients and for responders also an increase in fast alpha, while non-responders again showed the opposite effect. Ozaki et al. reported an increase in alpha in the electrodes C3/C4 and beta in the C3/C4 and P3/P4 electrodes [48]. Hughes et al. and Lee et al. examined healthy volunteers and compared the drug intake to a placebo. Mucci et al. on the other hand examined patients with schizophrenia before and after treatment. Ozaki et al. compared schizophrenic patients to healthy subjects.

Other studies found no significant changes when comparing individuals administered with risperidone against those receiving no medication, across both healthy [49] and schizophrenic [50] populations.

We could not obtain any studies that compared risperidone to other antipsychotic drugs. Overall, there exists a notable variability among studies investigating the impact of risperidone on EEG recordings, highlighting substantial inconsistencies in their findings. It is important to note that the studies' design and technical details differ majorly, and the reports are often incomplete. Additionally, many studies conducted on healthy individuals exclusively recruited young male participants, raising questions about the generalizability of the findings to the broader population. Therefore, the comparison can only serve as an indicator of the alignment of our results with state-of-the-art knowledge. One important factor contributing to the possible differences is that the reviewed studies had between 10 and 20 subjects. In contrast, utilizing the TUH EEG Corpus, we had on average 268 patients in each drug group ranging from 18 to 1951 patients. The largely increased number of subjects leads to an increased power of the statistical tests. Accordingly, we can detect significant changes for frequency bands, where previously no change was observed.

Another point that needs consideration is the differentiation between the drug-induced changes and the disease-induced ones. For instance, the review of Newson and Thiagarajan [51] on patients with schizophrenia suggests that some spectral EEG alterations may be attributed to the disease. The problem of this differentiation is also visible in the current state of the knowledge. Faiman and colleagues [52] reviewed the difference in EEG patterns between epilepsy patients and a control group. In most of the reviewed studies, patients were taking antiseizure drugs and only one study compared the changes in absolute powers between epilepsy patients who took no drugs and a healthy control group [53]. In the review of Yasin et al., it was investigated how bipolar disorder can be characterized using biomarkers in EEG measurements [54].

In our work, the results we obtained for Drug vs. "normal" also do not allow for the differentiation between the drug and disease effects. The benefit of comparing a single drug effect to the whole group arguably allows to partially remove the effect of the disease itself, though the specific drug usage can be potentially correlated to a certain subtype of the disease, and thus disease-linked EEG changes different from the general patient population.

4.3. Statistical considerations

The TUH EEG Corpus, characterized by its substantial sample size, plays a pivotal role in shaping the statistical evaluation within our pipeline. The large sample size inherently contributes to increased precision, thereby enhancing the reliability of estimates derived from the data. Moreover, it augments statistical power, empowering the pipeline to detect small effects that might be of clinical or scientific relevance, but would not be detected in smaller samples, providing a nuanced understanding of neurophysiological patterns. The generalizability of findings is bolstered, as the sample ensures that results are more likely to apply to the broader population, thereby enhancing external validity. Additionally, the large sample size facilitates robust replications and cross-validation of findings, reinforcing the reliability of the results. However, potential limitations associated with large sample sizes should be acknowledged, including the possibility of increased heterogeneity within the dataset due to diverse subpopulations. Additionally, the lack of detailed information on drug intake and diagnosis in this large-scale study presents a disadvantage when compared to smaller but well-controlled studies. Potential biases, such as selection and sampling biases where certain groups within the population are disproportionately represented can still be present in

large sample sizes and could affect the generalizability of the findings.

4.4. Limitations

We could not control all study parameters in our pipeline, since the metadata of the EEG files was in a semi-structured format with sections written in full text and possibly incomplete. The information provided was similar to a patient report and accordingly, it was not standardized with varying degrees of detail depending on the respective physician.

To improve the accessibility of the text reports and extract relevant metadata in future studies, various text extraction methods can be employed. While we have utilized regular expressions to extract patient medicine intake data, this approach encounters limitations when attempting to extract more nuanced information, such as medication dosage as an example. The variability and lack of standardization in text presentation within the text pose challenges. Therefore, alternative methods should be considered. Text parsing techniques, capable of breaking down unstructured text into structured data using predefined rules or grammar, present a promising avenue. Additionally, the application of machine learning models, particularly those rooted in natural language processing, offers an automated means of extracting information from text, leveraging labeled training data to discern patterns and nuances. These multifaceted approaches contribute to a more comprehensive and adaptable strategy for extracting intricate details from text reports.

The text reports include important technical details, such as the type of EEG equipment, the number of electrodes, and the electrode placement used during the recording of the EEG signals. An example of this can be found in Textbox 1 under the Section "Technique". However, it is worth noting that the EEG setup can vary among different patients, depending on factors such as the clinical indication for the EEG recording, the patient's age, and the EEG technician's preference.

Not all study parameters have the same importance for the EEG changes in the power spectrum. For example, sex, treatment response, length of hospital stay, drug potency, and dosage (apart from clozapine) do not seem to influence the EEG changes [41,55]. On the other hand, some diagnoses, such as high blood pressure or bipolar disorder, age, recording conditions, and pre-treatment state of the central nervous system influence the EEG changes significantly [55,56]. The nature of the database, constructed for the hospital-routine data, also limits the options for tracking the temporal development of the changes or the comparison to non-medication conditions for the same cohort.

4.5. Future work

While our study has provided valuable insights into the EEG profiles influenced by carbamazepine and risperidone, many more neuroactive drugs are present at high sample sizes in the TUH EEG Corpus that could be easily explored using the developed pipeline. An overview of those drugs is presented in Table A1. By understanding how various substances modulate brain activity, researchers can develop a more comprehensive framework for evaluating the neurological effects of different agents, thereby enhancing our understanding of brain functioning in diverse contexts.

Additionally, the TUH EEG Corpus provides the unique opportunity to investigate the interplay between different drugs, since many patients in the database take multiple drugs. Understanding how drugs interact with one another within the brain could provide insights into potential synergies or antagonisms. This knowledge is of importance in clinical settings where patients are often prescribed multiple medications simultaneously. Exploring these interactions could lead to more tailored and optimized drug regimens, minimizing adverse effects and maximizing therapeutic outcomes.

While the current study focused on the statistical analysis of the frequency bands, the pipeline could be easily adapted to analyze other important EEG-derived brain characteristics. For example, the recent study of Ishibashi et al. [57] shows the importance of brain connectivity studies in the research on drug-induced alterations. Since volume conduction [58] can confound the interpretation of connectivity measures, it would be important to add methods [59] to the pipeline that reduce this effect.

Due to the modularity of our pipeline, it can serve as a foundational framework for diverse machine learning projects, similar to other approaches using the TUH EEG Corpus, such as [28], where deep learning and feature-based approaches were compared that could classify EEG records regarding medication usage of the patient.

We encountered a significant challenge stemming from the unstructured nature of text reports describing EEG data and patient information, making access difficult. Enhancements to the pipeline could involve the implementation of novel methods to seamlessly integrate these text reports and automatically extract relevant data from them [60].

5. Conclusions

We successfully constructed and tested a computational pipeline for mining and analyzing EEG data combined with medication information from the TUH EEG Corpus. The advantage of this pipeline is that it can be adjusted to many different study designs through its modular setup.

When we investigated the EEG profiles of individuals with drug intake of carbamazepine or risperidone with the pipeline, our findings revealed a high level of consistency with existing literature, indicating the reliability of our results. The remaining differences could be explained by several factors. On the one hand, the large sample size provided by the TUH EEG Corpus provided hundreds to thousands of patients with intake of a certain drug and, thereby, enabled us to uncover nuanced effects that might be overlooked in smaller studies. This may lead to a more comprehensive understanding of the EEG alterations. On the other hand, the methods used in the literature varied significantly, rendering the generalization of drug effects across studies difficult. May studies reported the results only partially. The standardized, thorough, and automatic analysis of the EGG data in our pipeline could decrease such discrepancies and provide a more detailed characterization of the neural activity patterns influenced by neuroactive drugs while facilitating the analysis itself.

The results obtained in this study and future results generated using the computational pipeline can inform the design of controlled clinical trials. Further, the pipeline can be used for testing preliminary study concepts and estimating the necessary sample size. By facilitating a standardized drug examination and analysis of EEG patterns, the pipeline provides a valuable tool for advancing research and clinical trial design. Aligning with a long history of previous research the importance of EEG measurements to assess drug-induced changes in the brain is further supported by our results and the presented computational pipeline.

CRediT authorship contribution statement

Anna Maxion: Writing – review & editing, Writing – original draft, Visualization, Validation, Software, Formal analysis, Data curation. **Arnim Johannes Gaebler:** Writing – review & editing, Validation, Supervision, Methodology. **Rainer Röhrig:** Writing – review & editing, Validation, Supervision, Funding acquisition. **Klaus Mathiak:** Writing – review & editing, Validation, Supervision, Methodology, Conceptualization. **Jana Zweerings:** Writing – review & editing, Validation, Supervision, Methodology. **Ekaterina Kutafina:** Writing – review & editing, Supervision, Project administration, Methodology, Conceptualization.

Declaration of competing interest

None declared.

Acknowledgements

AM is funded by the Deutsche Forschungsgemeinschaft (DFG, German Research Foundation) – 368482240/GRK2416. AJG was funded by the Clinician Scientist Scholarship of the Medical Faculty of RWTH Aachen University.

Appendix

Table A1
Drug groups with corresponding drugs and their trade names, number of files downloaded and cleaned, as well as number of patients before and after outlier removal.

	drug	trade names	down-loaded files	cleaned files	patients	patients after outlier removal
Normal						
			1521	1521 w/o meds: 881	840	632
Group AP						
	Aripiprazole	Abilify, Abilify Maintena, Aristada, Aristada Initio	196	189	84	63
	Haloperidol	Haldol, Haldol Decanoate, haloperidol lactate	622	613	325	313
	Olanzapine	Zyprexa, Zyprexa Zydis, Zyprexa Relprevv, Zyprexa Intramuscular	218	174	83	82
	Quetiapine	Seroquel, Seroquel XR	788	777	315	267
	Risperidone	Risperdal, Risperdal Consta, Perseris, Risperdal M-Tab	946	392	84	62
	Ziprasidone	Geodon, Zeldox	53	50	32	19
Group CLZ						
	Clozapine	Clozaril, Clopine, FazaClo, Clozapine Synthon	64	62	22	18
Group AD						
	Bupropion	Wellbutrin, Wellbutrin XL, Wellbutrin SR, Zyban	120	119	59	37
	Escitalopram	Lexapro	295	284	111	72
	Fluoxetine	Prozac, Prozac Weekly, Sarafem, Rapiflux	568	377	152	146
	Mirtazapine	Remeron, Remeron SolTab	192	188	104	88
	Paroxetine	Paxil, Paxil CR, Brisdelle, Pexeva	220	217	111	110
	Sertraline	Zoloft, sertraline hydrochloride	638	614	265	263
	Trazodone	Desyrel, Oleptro, Desyrel Dividose	482	473	202	152
	Venlafaxine	Effexor XR, Effexor, venlafaxine hydrochloride	178	176	90	63
Group AS						
	Carbamazepine	Tegretol, Carbatrol, Tegretol XR, Epitol	2865	2315	348	302
	Lamotrigine	Lamictal, Lamictal XR, Subvenite, Lamictal ODT	2362	2147	520	510
	Levetiracetam	Elepsia XR, Keppra, Keppra XR, Roweepra, Spritam, Roweepra XR	13,339	12,275	2464	2136
	Topiramate	Topamax, Trokendi XR, Topamax Sprinkle, Qudexy XR	2842	2640	529	526
	Valproate	Valproate Sodium, Depakene, Depacon, Stavzor	481	471	175	170
Group Li						
	Lithium	Lithium Carbonate ER, Lithobid, Eskalith, Lithonate	68	68	33	30
Group BDZ						
	Alprazolam	Xanax, Xanax XR, Alprazolam Intensol, Niravam	777	753	303	281
	Clonazepam	Klonopin, Klonopin Wafer	1194	1154	331	272
	Diazepam	Valium, Valtoco, Diastat, Diastat AcuDial	379	371	153	145
	Lorazepam	Ativan, Lorazepam Intensol, Ativan Injection	7859	7520	1976	1951

References

[1] P.C. Casarotto, M. Girych, S.M. Fred, V. Kovaleva, R. Moliner, G. Enkavi, et al., Antidepressant drugs act by directly binding to TRKB neurotrophin receptors, Cell 184 (5) (2021) 1299–1313, e19.
[2] N. Mariani, J. Everson, C.M. Pariante, A. Borsini, Modulation of microglial activation by antidepressants, J. Psychopharmacol. Oxf. Engl. 36 (2) (2022)131–150.
[3] I. Esterlis, N. DellaGioia, R.H. Pietrzak, D. Matuskey, N. Nabulsi, C.G. Abdallah, et al., Ketamine-induced reduction in mGluR5 availability is associated with an antidepressant response: an [11C]ABP688 and PET imaging study in depression, Mol. Psychiatry 23 (4) (2018) 824–832.
[4] S.E. Holmes, S.J. Finnema, M. Naganawa, N. DellaGioia, D. Holden, K. Fowles, et al., Imaging the effect of ketamine on synaptic density (SV2A) in the living brain, Mol. Psychiatry 27 (4) (2022) 2273–2281.
[5] O.D. Howes, A. Egerton, V. Allan, P. McGuire, P. Stokes, S. Kapur, Mechanisms underlying psychosis and antipsychotic treatment response in schizophrenia: insights from PET and SPECT imaging, Curr. Pharm. Des. 15 (22) (2009) 2550–2559.
[6] G. Gründer, D.F. Wong, [The next generation of 'atypical' antipsychotics: the role of positron emission tomography], Fortschr. Neurol. Psychiatr. 71 (8) (2003) 415–420.
[7] F. Centorrino, B.H. Price, M. Tuttle, W.M. Bahk, J. Hennen, M.J. Albert, et al., EEG abnormalities during treatment with typical and atypical antipsychotics, Am. J. Psychiatry 159 (1) (2002) 109–115.
[8] J. Hyun, M.J. Baik, U.G. Kang, Effects of psychotropic drugs on quantitative eeg among patients with schizophrenia-spectrum disorders, Clin. Psychopharmacol. Neurosci. 9 (2) (2011) 78–85.
[9] S.M. Paul, W.Z. Potter, Finding new and better treatments for psychiatric disorders, Neuropsychopharmacology (2023) 1–7.
[10] A. Abi-Dargham, S.J. Moeller, F. Ali, C. DeLorenzo, K. Domschke, G. Horga, et al., Candidate biomarkers in psychiatric disorders: state of the field, World Psychiatry 22 (2) (2023) 236–262.
[11] S. Crüwell, J. van Doorn, A. Etz, M.C. Makel, H. Moshontz, J.C. Niebaum, et al., Seven easy steps to open science, Z. Psychol. 227 (4) (2019) 237–248.
[12] R. Vicente-Saez, C. Martinez-Fuentes, Open science now: a systematic literature review for an integrated definition, J. Bus. Res. 88 (2018) 428–436.
[13] M.D. Wilkinson, M. Dumontier, I.J. Aalbersberg, G. Appleton, M. Axton, A. Baak, et al., The FAIR Guiding Principles for scientific data management and stewardship, Sci. Data (2016) 3 [Internet][cited 2020 Sep 10]Available from: https://www.ncbi.nlm.nih.gov/pmc/articles/PMC4792175/.
[14] J. Wise, A.G. de Barron, A. Splendiani, B. Balali-Mood, D. Vasant, E. Little, et al., Implementation and relevance of FAIR data principles in biopharmaceutical R&D, Drug Discov. Today 24 (4) (2019) 933–938.

[15] S. Wiseman, A FAIR platform for data-sharing, Nat. Neurosci. 24 (12) (2021), 1640–1640.
[16] MIT Laboratory for computational physiology. PhysioNet [Internet]. [cited 2023 Apr 21]. Available from: https://physionet.org/.
[17] U.S. Department of Health and Human Services Office of the Chief Data Officer. Tyler Data & Insights. [cited 2023 Apr 21]. HealthData.gov. Available from: https://healthdata.gov/.
[18] Centers for Disease Control and Prevention, Chronic Disease Data, CDC, 2021 [Internet][cited 2023 Apr 21]. Available from: https://www.cdc.gov/chronicdisease/data/index.htm.
[19] World Health Organization. Data Collections - WHO [Internet]. [cited 2023 Apr 21]. Available from: https://www.who.int/data/collections.
[20] A. Harati, S. Choi, M. Tabrizi, I. Obeid, J. Picone, M.P. Jacobson, The temple university hospital EEG corpus, in: Proceedings of the IEEE Global Conference on Signal and Information Processing, 2013, pp. 29–32.
[21] I. Obeid, J. Picone, The temple university hospital EEG data corpus, Front. Neurosci. 10 (2016) [Internet][cited 2021 Mar 22]Available from: https://www.frontiersin.org/articles/10.3389/fnins.2016.00196/full.
[22] A. Brenner, E. Kutafina, S.M. Jonas, Automatic Recognition of Epileptiform EEG Abnormalities, Stud. Health Technol. Inform. (2018) 171–175.
[23] L.A.W. Gemein, R.T. Schirrmeister, P. Chrabąszcz, D. Wilson, J. Boedecker, A. Schulze-Bonhage, et al., Machine-learning-based diagnostics of EEG pathology, Neuroimage 220 (2020) 117021.
[24] M. Golmohammadi, A.H. Harati Nejad Torbati, S. Lopez de Diego, I. Obeid, J Picone, Automatic analysis of EEGs using big data and hybrid deep learning architectures, Front. Hum. Neurosci. 13 (2019) [Internet][cited 2023 Jan 18] Available from: https://www.frontiersin.org/articles/10.3389/fnhum.2019.00076.
[25] A. Harati, S. López, I. Obeid, J. Picone, M.P. Jacobson, S. Tobochnik, The TUH EEG CORPUS: a big data resource for automated EEG interpretation, in: Proceedings of the IEEE Signal Processing in Medicine and Biology Symposium (SPMB), 2014, pp. 1–5.
[26] S. Roy, I. Kiral-Kornek, S. Harrer, Deep learning enabled automatic abnormal EEG identification, in: Proceedings of the 40th Annual International Conference of the IEEE Engineering in Medicine and Biology Society (EMBC), 2018, pp. 2756–2759.
[27] İ. Yıldız, R. Garner, M. Lai, D. Duncan, Unsupervised seizure identification on EEG, Comput. Methods Programs Biomed. 215 (2022) 106604.
[28] D.O. Nahmias, E.F. Civillico, K.L. Kontson, Deep learning and feature based medication classifications from EEG in a large clinical data set, Sci. Rep. 10 (1) (2020) 14206.
[29] Temple University EEG Corpus [Internet]. [cited 2023 Apr 28]. Available from: https://isip.piconepress.com/projects/tuh_eeg/index.shtml.
[30] S. Roy, I. Kiral, M. Mirmomeni, T. Mummert, A. Braz, J. Tsay, et al., Evaluation of artificial intelligence systems for assisting neurologists with fast and accurate annotations of scalp electroencephalography data, EBioMedicine 66 (2021) [Internet][cited 2023 Apr 28], https://www.thelancet.com/journals/ebiom/article/PIIS2352-3964(21)00068-2/fulltext.
[31] rwth-imi/Drug_induced_spectral_changes_TUH, RWTH Aachen University Institute of Medical Informatics, 2022 [Internet][cited 2023 Jan 25]. (Drug induced spectral changes TUH). Available from: https://github.com/rwth-imi/Drug_induced_spectral_changes_TUH.
[32] A. Delorme, S. Makeig, EEGLAB: an open source toolbox for analysis of single-trial EEG dynamics including independent component analysis, J. Neurosci. Methods 134 (1) (2004) 9–21.
[33] S. López, G. Suarez, D. Jungreis, I. Obeid, J. Picone, Automated identification of abnormal adult EEGs, IEEE Signal Process. Med. Biol. Symp. 2015 (2015), https://doi.org/10.1109/SPMB.2015.7405423.
[34] S. López, G. Suarez, D. Jungreis, I. Obeid, J. Picone, Automated Identification of Abnormal Adult EEGs, IEEE Signal Process. Med. Biol. Symp. SPMB 2015 (2015).
[35] Ferrell S., Mathew V., Refford M., Tchiong V., Ahsan T., Obeid I., et al. The neural engineering data consortium college of engineering, Temple University 1947 North 12th Street Philadelphia, Pennsylvania 19122 Tel: 215-204-4841; Fax: 215-204-5960 Email: {sean.ferrell, vineetha.mathew, matthew.refford, vincent.tchiong, tameem.ahsan, iobeid, picone}@temple.edu. 2020.
[36] C.Y. Chang, S.H. Hsu, L. Pion-Tonachini, T.P. Jung, Evaluation of artifact subspace reconstruction for automatic artifact components removal in multi-channel EEG recordings, IEEE Trans. Biomed. Eng. 67 (4) (2020) 1114–1121.
[37] M. Schmidt, P. Kanda, L. Basile, H. da Silva Lopes, R. Baratho, J. Demario, et al., Index of alpha/theta ratio of the electroencephalogram: a new marker for Alzheimer's disease, Front. Aging Neurosci. 5 (2013) [Internet][cited 2022 Dec 20] Available from: https://www.frontiersin.org/articles/10.3389/fnagi.2013.00060.
[38] A. Jaramillo-Jimenez, J.X. Suarez-Revelo, J.F. Ochoa-Gomez, J.A. Carmona Arroyave, Y. Bocanegra, F. Lopera, et al., Resting-state EEG alpha/theta ratio related to neuropsychological test performance in Parkinson's Disease, Clin. Neurophysiol. 132 (3) (2021) 756–764.
[39] A.L. Lamprecht, L. Garcia, M. Kuzak, C. Martinez, R. Arcila, E. Martin Del Pico, et al., Towards FAIR principles for research software, Data Sci. 3 (1) (2020) 37–59.
[40] M.G. Marciani, G.L. Gigli, M.C.E. Maschio, N. Stefani, F. Stefanini, G. Bernardi, EEG changes induced by carbamazepine therapy at rest and during mental processes, Ital. J. Neurol. Sci. 13 (9) (1992) 729–733.
[41] R. Besser, K. Hornung, M. Theisohn, G. Rothacher, G. Krämer, EEG changes in patients during the introduction of carbamazepine, Electroencephalogr. Clin. Neurophysiol. 83 (1) (1992) 19–23.
[42] O. Mecarelli, E. Vicenzini, P. Pulitano, N. Vanacore, F.S. Romolo, V.D. Piero, et al., Clinical, cognitive, and neurophysiologic correlates of short-term treatment with carbamazepine, oXcarbazepine, and levetiracetam in healthy volunteers, Ann. Pharmacother. 38 (11) (2004) 1816–1822.
[43] J.D. Frost, R.A. Hrachovy, D.G. Glaze, G.M. Rettig, Alpha rhythm slowing during initiation of carbamazepine therapy: implications for future cognitive performance, J. Clin. Neurophysiol. Off. Publ. Am. Electroencephalogr. Soc. 12 (1) (1995) 57–63.
[44] X. Wu, C.H. Xiao, Quantitative pharmaco-EEG of carbamazepine in volunteers and epileptics, Clin. Electroencephalogr. 27 (1) (1996) 40–45.
[45] A. Mucci, U. Volpe, E. Merlotti, P. Bucci, S. Galderisi, Pharmaco-EEG in psychiatry, Clin. EEG Neurosci. 37 (2) (2006) 81–98.
[46] A.M. Hughes, P. Lynch, J. Rhodes, C.M. Ervine, R.A. Yates, Electroencephalographic and psychomotor effects of chlorpromazine and risperidone relative to placebo in normal healthy volunteers, Br. J. Clin. Pharmacol. 48 (3) (1999) 323–330.
[47] D.Y. Lee, K.U. Lee, J.S. Kwon, I.J. Jang, M.J. Cho, S.G. Shin, et al., Pharmacokinetic-pharmacodynamic modeling of risperidone effects on electroencephalography in healthy volunteers, Psychopharmacology 144 (3) (1999) 272–278.
[48] T. Ozaki, A. Toyomaki, N. Hashimoto, I. Kusumi, Quantitative resting state electroencephalography in patients with schizophrenia spectrum disorders treated with strict monotherapy using atypical antipsychotics, Clin. Psychopharmacol. Neurosci. Off. Sci. J. Korean Coll. Neuropsychopharmacol. 19 (2) (2021) 313–322.
[49] H. Allain, C. Tessier, D. Bentue-Ferrer, A. Tarral, S. Le Breton, J. Gandon, et al., Effects of risperidone on psychometric and cognitive functions in healthy elderly volunteers, Psychopharmacology 165 (4) (2003) 419–429 (Berl).
[50] B. Tislerova, M. Brunovsky, J. Horacek, T. Novak, M. Kopecek, P. Mohr, et al., LORETA functional imaging in antipsychotic-naive and olanzapine-, clozapine- and risperidone-treated patients with schizophrenia, Neuropsychobiology 58 (1) (2008) 1–10.
[51] J.J. Newson, T.C. Thiagarajan, EEG frequency bands in psychiatric disorders: a review of resting state studies, Front. Hum. Neurosci. 12 (2019) [Internet][cited 2022 Dec 2]Available from: https://www.frontiersin.org/articles/10.3389/fnhum.2018.00521.
[52] I. Faiman, S. Smith, J. Hodsoll, A.H. Young, P. Shotbolt, Resting-state EEG for the diagnosis of idiopathic epilepsy and psychogenic nonepileptic seizures: a systematic review, Epilepsy Behav. 121 (2021) 108047.
[53] B. Clemens, Valproate decreases EEG synchronization in a use-dependent manner in idiopathic generalized epilepsy, Seizure Eur. J. Epilepsy 17 (3) (2008) 224–233.
[54] S. Yasin, S.A. Hussain, S. Aslan, I. Raza, M. Muzammel, A. Othmani, EEG based major depressive disorder and bipolar disorder detection using neural networks:a review, Comput. Methods Programs Biomed. 202 (2021) 106007.
[55] R. Aiyer, V. Novakovic, R.L. Barkin, A systematic review on the impact of psychotropic drugs on electroencephalogram waveforms in psychiatry, Postgrad. Med. 128 (7) (2016) 656–664.
[56] B. Saletu, P. Anderer, G.M. Saletu-Zyhlarz, EEG topography and tomography (LORETA) in the classification and evaluation of the pharmacodynamics of psychotropic drugs, Clin. EEG Neurosci. 37 (2) (2006) 66–80.
[57] T. Ishibashi, S. Nobukawa, M. Tobe, M. Kikuchi, T. Takahashi, Alterations in the hub structure of whole-brain functional networks in patients with drug-naïve schizophrenia: insights from electroencephalography-based research, Psychiatry Clin. Neurosci. Rep. 3 (1) (2024) e164.
[58] S.P. van den Broek, F. Reinders, M. Donderwinkel, M.J. Peters, Volume conduction effects in EEG and MEG, Electroencephalogr. Clin. Neurophysiol. 106 (6) (1998) 522–534.
[59] C. Brunner, M. Billinger, M. Seeber, T.R. Mullen, S. Makeig, Volume conduction influences scalp-based connectivity estimates, Front. Comput. Neurosci. 10 (2016) [Internet][cited 2024 May 13]Available from: https://www.frontiersin.org/articles/10.3389/fncom.2016.00121.
[60] L. Marinelli, C. Cabona, I. Pappalardo, A. Bellini, A. Ferrari, E. Micalizzi, et al., Tagging EEG features within exam reports to quickly generate databases for research purposes, Comput. Methods Programs Biomed. 242 (2023) 107836.

Acknowledgments

I would like to thank my supervisor, Prof. Dr. Barbara Namer, who guided me through all phases of this work with her expertise, constructive feedback, and support. Without her knowledge and valuable advice, this work would not have been possible.

I am grateful to Dr. Ekaterina Kutafina who first introduced me to this project and opened the doors to many connections and opportunities along the way. Without her guidance and encouragement, I might never have embarked on this PhD journey. Her support has been fundamental to my progress and success.

I am also appreciative of Prof. Dr. Jenny Tigerholm for her support throughout this project. Her insights, encouragement, and willingness to help whenever needed made a significant difference in my work and progress. I am grateful for her guidance during this journey.

I extend my thanks to my doctoral supervisor, Prof. Dr. Angelika Lampert, for the opportunity to carry out this PhD project within her research group.

I wish to acknowledge my research training group RTG2416 MultiSenses – MultiScales for their support and community throughout my PhD journey. The retreats and training sessions organized by the group enriched my research experience, and the financial support to attend conferences provided me with opportunities to present my work and connect with others in the field.

I would like to thank my colleagues Andrea Fiebig, Alina Troglio, Danxia Bao and Dr. Stas Koulchitsky for their support, collaboration, and encouragement throughout my PhD journey. Working alongside such talented people has been a source of inspiration and motivation. I appreciate the discussions, feedback, and team spirit we shared.

To my husband and kids, I would like to express my gratitude for their support, love, and encouragement throughout this journey. Your patience and understanding have been my source of strength, and I am incredibly grateful for the joy you bring into my life. Thank you for believing in me and standing by my side every step of the way.

I would like to express my gratitude to my parents and family for their contributions to my journey. Your support has helped shape who I am today, and I appreciate the role you have played in my development. Thank you for being a part of this significant milestone in my life.

Erklärung § 5 Abs. 1 zur Datenaufbewahrung

Hiermit erkläre ich, dass die dieser Dissertation zu Grunde liegenden Originaldaten bei meiner Betreuerin

Prof. Dr. Barbara Namer
Zentrum für interdisziplinäre Schmerzmedizin
Straubmühlweg 2a/Haus A9,
97078 Würzburg

hinterlegt sind.

Erklärung gemäß § 5 Abs. (1) und (2), und § 11 Abs. (3) 12. der Promotionsordnung

Hiermit erkläre ich, **Anna Maxion,** an Eides statt, dass ich den wesentlichen Anteil an der Publikation:

Anna Maxion, Ekaterina Kutafina, Maike Dohrn, Pierre Sacré, Angelika Lampert, Jenny Tigerholm, Barbara Namer**:** A modelling study to dissect the potential role of voltage-gated ion channels in activity-dependent conduction velocity changes as identified in small fiber neuropathy patients; Frontiers in Computational Neuroscience; 2023, Volume 17:1265958, geleistet habe.
Die Anteile an der Arbeit waren wie folgt:

	Anna Maxion	Ekaterina Kutafina	Maike Dohrn	Pierre Sacré	Angelika Lampert	Jenny Tigerholm	Barbara Namer	Summe (%)
Konzeption/Supervision		15		5		40	40	100
Methodik/ Validierung		10			35	15	40	100
Datenkuratierung/Materialien			15				85	100
Formale Analyse	100							100
Software	100							100
Visualisierung	100							100
Verfassung des Manuskripts	100							100
Korrektur des Manuskripts	14	14	14	14	14	15	15	100

Aus diesem wesentlichen Anteil ergibt sich selbstverständlich die Stellung als Erstautor / in.

_____

Anna Maxion

Als Doktormutter und / oder korrespondierende Autoren bestätige ich die Angaben von Anna Maxion und in Vertretung für den Kooperationspartner Pierre Sacré.

_____ _____ _____

Angelika Lampert Barbara Namer Jenny Tigerholm

Ich schließe mich der Erklärung von Angelika Lampert als Koautor an

_____

Ekaterina Kutafina

_____

Maike Dohrn

Erklärung gemäß § 5 Abs. (1) und (2), und § 11 Abs. (3) 12. der Promotionsordnung

Hiermit erkläre ich, **Anna Maxion,** an Eides statt, dass ich den wesentlichen Anteil an der Publikation:

Anna Maxion, Arnim Johannes Gaebler, Rainer Röhrig, Klaus Mathiak, Jana Zweerings, and Ekaterina Kutafina**:** Spectral changes in electroencephalography linked to neuroactive medications: a computational pipeline for data mining and analysis; Computer Methods and Programs in Biomedicine; 2024, Volume 255 geleistet habe.

Die Anteile an der Arbeit waren wie folgt:

	Anna Maxion	Arnim Johannes Gaebler	Rainer Röhrig	Klaus Mathiak	Jana Zweerings	Ekaterina Kutafina	Summe (%)
Studiendesign, -überwachung, Bereitstellung von Materialien		15	15	15	15	40	100
Datenauswertung	100						100
Statistische Auswert.	70	10		10	10		100
Interpretation der Datenauswertung	40	10	5	10	10	25	100
Verfassung des Manuskripts	100						100
Korrektur des Manuskripts		15	10	10	20	45	100

Aus diesem wesentlichen Anteil ergibt sich selbstverständlich die Stellung als Erstautor / in.

_____

Unterschrift der Doktorandin/des Doktoranden

Als Doktormutter und / oder korrespondierender Autor bestätige ich die Angaben von Anna Maxion.

_____ _____

Angelika Lampert Ekaterina Kutafina

Ich schließe mich der Erklärung von Angelika Lampert als Koautor an

_____

Arnim Johannes Gaebler

_____

Rainer Röhrig

_____

Klaus Mathiak

_____

Jana Zweerings